Hydrology and quantitative water management group

MSc Thesis

Entropy and river meander planform

Adriaan J. Teuling

August 2002

Supervisor: Prof. Peter A. Troch

K150-711

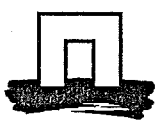

WAGENINGEN UNIVERSITY
ENVIRONMENTAL SCIENCES

ENTROPY AND RIVER MEANDER PLANFORM

ADRIAAN J. TEULING

MSc student, Wageningen University, The Netherlands

ABSTRACT: This study departs from the hypothesis that the often striking geometric similarity and regularity of meanders is the result of the second law of thermodynamics applied to open dissipative systems. It is argued that along a meandering river the continuous production of entropy is as low and as uniform as possible. An expression of entropy production in a moderately meandering river is derived. A dimensionless form of Odgaard's Meander flow model (1986*a*) is used to evaluate this expression along different meander bends described by the class of third order sine-generated curves. The results show a minimum variance of entropy production for a fattened curve with upvalley skewing, indicating that meander asymmetry described by Carson and Lapointe (1983) is in correspondence with the Theory of minimum variance (Langbein and Leopold, 1966).

It is pleasant to have been to a place the way a river went.
- *Henry David Thoreau (1817-1862)*

I. INTRODUCTION

The typical winding path of lowland rivers raised the interest of many scientists, amongst whom famous scientists as Lord Kelvin (1876) and Einstein (1926). This winding, named meandering after the river Büyükmenderes in Turkey, is shown in Figure 1. The absence of straight reaches in natural rivers indicates that meandering is inherent to the flow processes in a river. Although extensive research throughout the past decades has lead to a good understanding of these processes, one of the most intriguing questions is still unanswered, namely why do different meanders often exhibit the same shape regardless of scale? In this paper a physical explanation is proposed.

Figure 1. Meandering river (source unknown).

Meandering is not restricted to natural rivers or fixed boundaries. Meanders have also been reported in laboratory conditions (Langbein and Leopold, 1966, Schumm et al., 1972, Smith, 1998), ocean currents (Leopold, 1995, his Figure 4.5, Ikeda et al., 1989), water rivulets on glass plates (Mizumura and Yamasaka, 1997), supraglacial streams (Ferguson, 1973, Dozier, 1976), solution channels in limestone (Jennings, 1972, p. 45), density current (Leopold, 1995, his Figure 4.6) and even in lava channels on Venus (Komatsu and Baker, 1994). All these meanders show remarkable geometric similarity over a wide range of scales (Figure 2, Leopold, 1995, his Figure 4.2, Davy and Davies, 1979, their Figure 1). This suggests that the typical meander planform is the result of a physical principle. In this paper it will be shown that the typical meander planform is the result of the thermodynamic principle of maximum entropy. In the following section a review is given of the existing planform theories and at the same time some basic terms will be introduced. In Section III the consequences of the maximum entropy principle for a river system will be discussed and an expression of entropy production in a meandering river is derived. The velocity gradients in this expression are determined with a flow model for meandering rivers described in Section IV. The results are presented in Section V and discussed in Section VI.

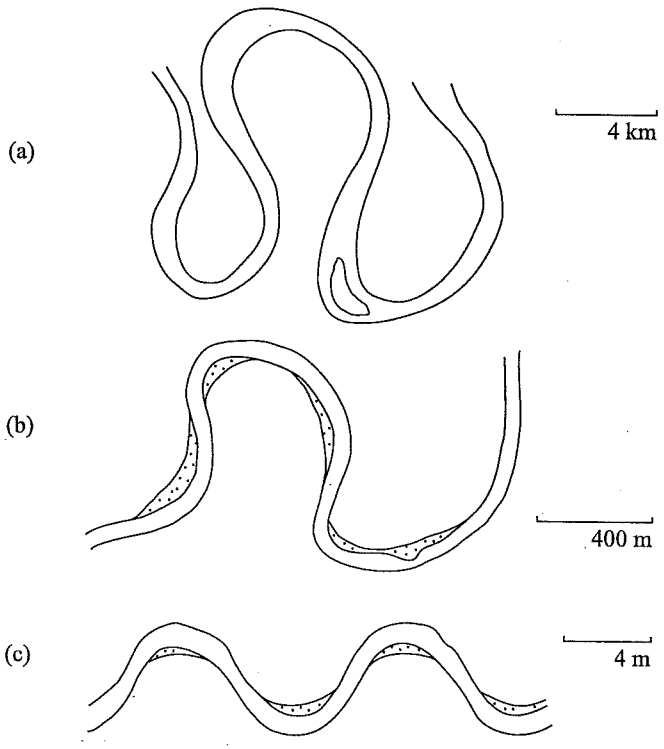

Figure 2. Examples of river meanders of different scale and sinuosity. (a) Mississippi River at Greenville, Miss., USA, before

the artificial cutoffs (redrawn after Langbein and Leopold, 1966), (b) White River at Edwardsport, Ind., USA (redrawn after Brice, 1974), (c) Laboratory meander (redrawn after Langbein and Leopold, 1966). In all cases flow is from left to right. Shade indicates bars (b) or shoal areas (c).

II. Review of planform theories

In 1869, Fargue made one of the first attempts known by the author to describe meander planform. He argued that rivers have one essential property, namely "la continuité de la variation de la courbure" (the continuity of the change in curvature) and that the curvature could thus be well described by a cosine function of the phase along the river (Flamant, 1891, p. 318). Unfortunately, in spite of the similarities with later theories, his findings stayed largely unknown. As part of a research on meander belts, Jefferson (1902) argued that meandering is the result of a minimization of energy, and that "maturely meandering streams may be regarded as finding their slope too steep". This implicates that rivers should develop towards a state of minimum slope and thus towards a minimum dissipation of energy, in correspondence to later findings.

In the 1960's Langbein and Leopold made important progress in the research on meandering. They derived many empirical relations for meandering rivers. One of the most used is the almost linear relationship between the width w of a river and the meander wavelength λ (Hey, 1976, see also Figure 3):

$$\lambda = 10.9 w^{1.01} \text{ feet} \tag{1}$$

Davy and Davies (1979) showed this relationship to be valid over seven orders of magnitude for different types of meanders. From these relations they showed that the ratio of minimum radius of curvature to width is almost constant for any meander (namely 2.4), roughly corresponding to the same ratio in bended pipes for which minimum energy losses occur. Langbein and Leopold (1966) also found that the path of a meander was very similar to the most probable path of a random walk of given length between two fixed points and therefore concluded that the meander path must somehow reflect a state of maximum likelihood. The most probable path for a random walk can be well described by a sine-generated curve (Langbein and Leopold, 1966), a curve in which $\Theta(s)$, the angle between the tangent to the curve and the downvalley x-axis, is a function of the phase ϕ along the curve:

$$\Theta(s) = \Theta_0 \cos\phi \tag{2}$$

in which $\phi = 2\pi s / L$ with s the coordinate along the curve and L the meanderlength measured along the curve; Θ_0 is the starting angle at $s = 0$ (see Figure 3). An example of a sine-generated curve is given in Figure 3. The sine-generated curve has another important property, namely it minimizes the sum of the squares of the changes in direction. This was the basis of the so-called Theory of minimum variance, stating that meanders are characterized by a minimum variance not only of angular deflection but also in hydraulic properties. Leopold and Langbein (1966) also argued that the Theory of minimum variance should perhaps be interpreted as a strive to uniformity in the rate of energy expenditure, but they provided no prove for this hypothesis. This implicates that the most probable path of a meander is the result of flow processes and is not necessarily a sine-generated curve, but this implication was never noted.

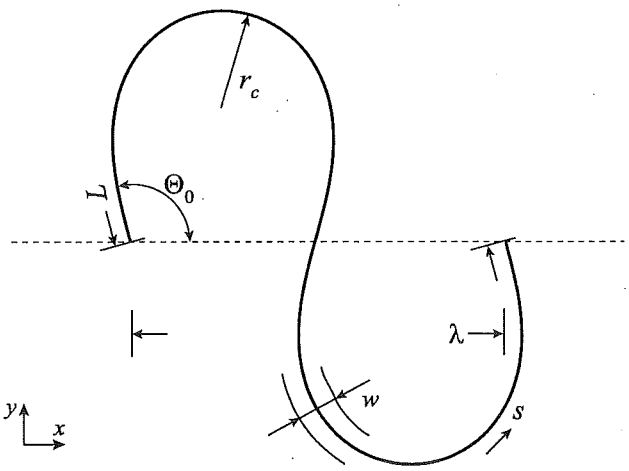

Figure 3. Sine-generated curve and definition of parameters.

In spite of the elegance of the Theory of minimum variance, the sine-generated curve proved to be an oversimplification of the meander planform, for the theory did not account for the two most important features in meandering rivers: namely bed topology (the bar-deep pool sequence) and helical motion. Though the sine-generated curve is still widely used to describe meander planform, Carson and Lapointe (1983) concluded after a statistical analysis of a large number of meandering rivers that the most probable meander bends possess two types of asymmetry, namely a delayed inflection and an upvalley skew in the meander loop, and that "the Theory of minimum variance should thus be abandoned". Based on the work of Ikeda et al. (1981) and Parker et al. (1982), Parker et al. (1983) provided a theoretical basis for the observed asymmetry in high amplitude meanders. They combined the dynamic description of flow in bends with a kinematic description of bank erosion, which resulted in the formulation of a more general function to describe meander planform. This function add skewing and fattening to the curve given by Equation 2:

$$\Theta(s) = \Theta_0 \cos\phi - \Theta_0^{\,3}\left(c_f \cos 3\phi + c_s \sin 3\phi\right) \tag{3}$$

in which c_f and c_s are parameters defining the amount of fattening respectively skewing of the sine-generated curve of equation 2. Different combinations of these parameters lead to a wide range of curves, from nearly sinuous to

circular or parabolic (see Figure 4). Parker et al. (1983) named this curve the "Kinoshita curve", but here the name third order sine-generated curve as used by Mizumura and Yamasaka (1997) will be used. Parker et al. (1983) found a curve with a negative fattening and upvalley skewing to best describe the "ideal state" of a meander.

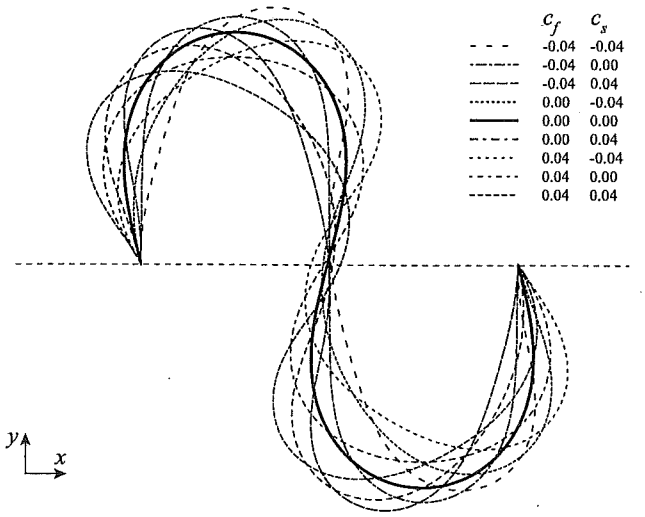

Figure 4. First order sine-generated curve compared with third order sine-generated curves of the same sinuosity, having different combinations of the fattening and skewing parameters.

The mechanistic bend equation used by Parker et al. (1983) formed the basis of several simulation models for meandering rivers (Howard and Knutson, 1984, Crosato, 1990, Sun et al., 1996, 2001a, 2001b, Meakin et al., 1996). Other models have only recently been developed (Lancaster and Bras, 2002), illustrating the still existing need to fully understand the process of meandering. Although these models are capable of simulating large scale meandering behavior, they do not offer a fundamental explanation for the characteristic planform of meandering rivers.

Little research has been done on the large-scale pattern of meandering. Stølum (1996, 1998) analyzed extended meander systems in the Amazon basin and concluded that meander systems possess fractal geometry and therefore must be the result of a process of self-organization. The state of a meander system can be expressed by the dimensionless parameter sinuosity (k), defined as:

$$k = \frac{L}{\lambda} \tag{4}$$

in which L and λ are defined in Figure 3. Local sinuosity ranges from an arbitrary minimum of 1.5 (Chang, 1984) to a theoretical maximum of 5.48 for circular bends (Chitale, 1973). It was shown by Stølum (1996) that through enlargement of meander bends and the opposing process of cut-off, the meander system develops into a steady state of self-organized criticality, which is characterized by fluctuations around an average sinuosity of π. This showed true for both field data and the Howard and Knutson model (1984). In the following section the steady state of a meander system will be discussed in terms of entropy.

III. The Concept of Entropy in Meandering Rivers

Irreversibility and probability

In natural processes, mechanical work is transferred into heat due to friction. Although work and heat are both terms of energy, it is easier to create heat out of work than it is to create work out of heat. This irreversibility can also be seen in the absence of work, since heat can only be transported from higher temperatures to lower. This implicates that processes possess a time-asymmetry and develop towards a state of disorder or dissipation of potentials. Order or potential can only be created by the input of energy. It can be seen that this disorder can be expressed in terms of energy, temperature, information or probability. In 1854 Clausius introduced the term entropy as a measure of the dissipated potential. In thermodynamics, the change in entropy S between two states A and B is defined as the integral of the ratio of change in internal energy E_i and absolute temperature T (Ohanian, 1989, p. 556):

$$S_B = S_A + \int_A^B \frac{dE_i}{T} \tag{5}$$

Equation 5 thus forms the link between entropy and energy. Other expressions of entropy in terms of probability and information were introduced by Boltzmann in 1872 and Shannon in 1948, but as this paper only deals with thermodynamic entropy they will not be described here. Although equation 5 forms the link between entropy and energy, it does not offer an explanation for the phenomenon of irreversibility. The second law of thermodynamics states that the entropy of a closed system must always increase or stay the same. Therefore this law defines the direction of time (time-asymmetry) in natural processes (Ohanian, 1989, p. 562):

$$S_B - S_A \geq 0 \tag{6}$$

The classical approach of entropy in closed systems cannot be used in open systems. In a closed system entropy will increase until equilibrium is reached at maximum entropy, while in open systems boundary conditions can prevent the system from reaching this equilibrium state. In this case entropy is continuously being generated. It was discovered by Prigogine in 1945 that linear thermodynamic systems close to equilibrium evolve "toward a stationary state characterized by the minimum entropy production compatible with the constraints imposed upon the system" (Prigogine and Stengers, 1985, p. 138). As steady state implies independence of time, the entropy of a system in steady state is also a constant and therefore the internal production of entropy is balanced by the rate of outflow of

entropy (Denbigh, 1951, p. 40). Thus the most probable state to which an open system evolves (corresponding to maximum entropy) is one in which the production of entropy is minimized. If the properties of a system are constant and independent of place (homogenous system), the system will evolve towards a state in which entropy production has the same minimum value in the whole system. For a homogenous system at maximum entropy, this also implicates a uniform, or at least as uniform as possible, distribution of entropy production.

Entropy and fluvial geomorphology

Assuming a constant discharge, a river can be considered as an open system in a steady state (Leopold, 1995, p. 57). This approach has been used before in fluvial geomorphology to explain other phenomena (Leopold and Langbein, 1962, Woldenberg, 1966). In a river a potential (gravitational or potential energy) is continuously converted into kinetic (ordered) energy. As this process is reversible (the gain in velocity for all molecules is in the same direction), this does not lead to an increase in entropy. The kinetic energy is converted into heat by friction in the fluid. As heat represents disordered energy (random motion of molecules), this process is irreversible and entropy increases.

One might wonder where this continuous increase in entropy is compensated, as the entropy of the earth as a whole does not seem to change. As order can only be created by the input of energy, it can be seen that the increase in entropy is balanced on a global scale by an increase in order caused by the input of solar radiation. This radiation provides the energy necessary for evaporation of water molecules and precipitation on a location with higher gravitational energy (hydrological cycle).

Because rivers adjust their course by the process of erosion and sedimentation, it is likely that this process is driven by an increase in entropy (equation 5). It is assumed that, under ideal circumstances (constant discharge, uniform valley slope and without cutoff's), rivers evolve towards a stationary state in which no more change in course takes place and where meander bends have a regular shape. Davies and Tinker (1984) found that surface tension meanders indeed evolve towards such a steady state and they argued that this should also be true for river meanders, although natural river meanders may never reach this steady state due to a continuously change of boundary conditions and stochastic variables like discharge. The tendency of meanders to evolve towards a steady state was confirmed by simple qualitative experiments with surface tension meanders on an inclined Perspex plate. A regular and stable surface tension meander is shown in Figure 5. Although there are major differences between surface tension meanders and river meanders, there was no evidence found in literature that these meanders behave differently.

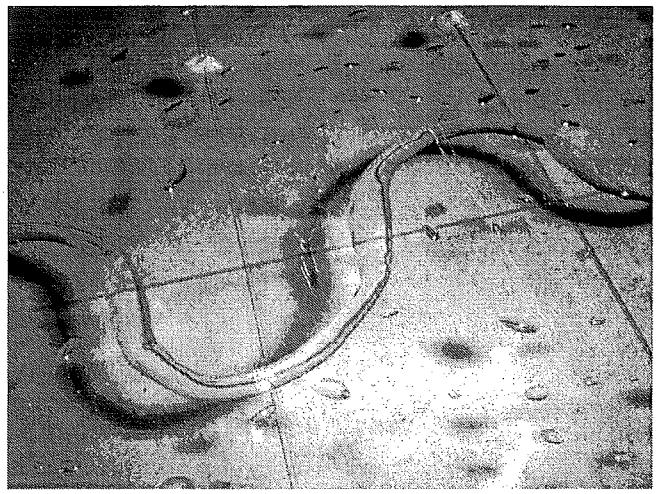

Figure 5. Stable surface tension meander. Flow is from left to right. (photograph by author)

The tendency of meanders to evolve towards a steady state might however no longer be true for meanders with high sinuosity's (>5). Above this value cutoff's are likely to occur and the self-organized nature of this process (Stølum, 1996) indicates that this process is no longer determined by an increase in entropy and will not reach an equilibrium state. It has been shown by Schumm et al. (1972) and Nagakawa and Scott (1984) that sinuosity is mainly determined by valley slope. In this research therefore focus is laid on rivers on relatively flat slopes with sinuosity's of less than 5, where no cutoff's take place. As the process of valley slope adjustment acts on a much larger timescale than the process of course adjustment, it is assumed that a river can reach an equilibrium state for any sinuosity, and that the sinuosity is determined by external factors as discharge, valley slope and sediment characteristics. The principle that rivers develop towards a state of maximum entropy corresponds to the conclusions reached by Song (1992) that "energy dissipation has been shown to be the primary stabilizing force that determines the direction of change towards an equilibrium condition". This minimization principle for natural rivers was the basis for the Theory of minimum rate of energy dissipation (Yang and Song, 1979).

At maximum entropy, the production of internal energy (heat, or entropy) is as low as possible. Davy and Davies (1979) concluded that strictly speaking the principle found by Prigogine is only derived for linear systems, and that minimum entropy production correspond to laminar flow. From analysis of surface tension meanders Davies and Tinker (1984) and Mizumura (1993) concluded that the typical meander shape is also present in laminar flow. Therefore the flow conditions seem of little importance to the applicability of the principle of minimum entropy production. Furthermore it was shown by Yang (1979) that

the same principle can also be derived from the Navier-Stoke's equation for turbulent flow. It is thus believed that Prigogine's principle not only determines the flow in a meander bend on a timescale smaller than the timescale at which changes bend shape take place, but that this principle also determines the changes in bend shape on a much larger timescale.

A first indication that meandering rivers correspond to a state of maximum entropy is given by considering the entropy production for different types of rivers. This parameter is generally the lowest for meandering rivers and has been applied successfully in several studies to distinguish between meandering and braiding rivers (Chang, 1979, Van den Berg, 1995, Lewin and Brewer, 2001). From experimental and Mississippi River data, Schumm et al. (1972) concluded that meandering occurs on smaller slopes. All these findings indicate that meandering and minimum entropy production are inherent phenomena.

Because a river system can be considered homogenous over relatively short distances (no change in constraints of discharge and sediment characteristics), a minimum entropy production will also result in a uniform entropy production along the river. However, the constraint of the presence of bends in a river and the associated helical motion implicates a non-uniform entropy production. It that case the most probable distribution of entropy production is one in which the distribution is as uniform as possible (Yang, 1971) or the variance of the entropy production is minimum (Langbein and Leopold, 1966). In this research the widely accepted minimum variance principle will be used. Minimization and uniformity of energy dissipation have also been used recently by Molnár and Ramírez (1998) and Huang and Nanson (2000) to explain hydraulic and geometric properties of rivers. In the following section an expression for entropy production along a meandering river is derived, which will then be used to determine the most probable meander planform.

Entropy production in a meandering river

With the assumption that the most probable planform for a meander bend reflects minimum variance of the entropy production, the question remains how to quantify this production of entropy? In an isothermal system the entropy production is solely caused by irreversible friction losses within the fluid. For incompressible fluids, the entropy production per unit volume and unit time, σ, is described by (Yang, 1992):

$$T\sigma = -(\tau : \nabla v) \tag{7}$$

in which T is the absolute temperature, τ is the stress tensor and v is the velocity vector. Equation 7 can be obtained by combining the first law of thermodynamics with the equation of motion for an isothermal system and incompressible fluid. Written in terms of energy, this derivation can be found in many handbooks on fluid mechanics (such as Bird et al., 1960, p. 313). This is shown in Appendix I. It is assumed that the stress tensor for turbulent flow in a river can be written in terms of a rate of strain tensor and a kinematic eddy viscosity, ε, similar to the kinematic viscosity in laminar flow. This implicates that the influences of turbulent flow on the meander planform is neglected. Smith and McLean (1984) and Odgaard (1986a) also used this assumption. The stress tensor can then be written in Einstein notation as:

$$\tau_{ij} = -2\rho\varepsilon\psi_{ij} \tag{8a}$$

in which ρ the density of the fluid and ψ_{ij} the rate of strain tensor. The rate of strain tensor is given by:

$$\psi_{ij} = \frac{1}{2}\left(\nabla v_{ij} + \nabla v_{ji}\right) \tag{8b}$$

in which i and j represent the directions s, n and z. The components of the rate of strain tensor follow from equation 7. For convenience, the velocity gradient tensor will be expressed in a right-handed, orthogonal, curvilinear coordinate system with a downstream s-axis, a cross-stream n-axis and a vertical z-axis (Figure 3, 6 and AII-1). The physical (Cartesian) space and the computational space resulting from the transformation of Cartesian into curvilinear coordinates are illustrated in Figure 6.

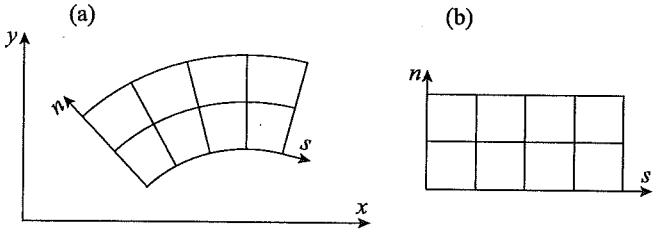

Figure 6. Illustration of coordinate transformation. (a) Physical space. (b) Computational space.

In curvilinear coordinates, the velocity gradient tensor is given by:

$$\nabla v_{ij} = \begin{bmatrix} \frac{1}{1-N}\frac{\partial v_s}{\partial s} - \frac{v_n}{r_c - n} & \frac{v_s}{r_c - n} + \frac{1}{1-N}\frac{\partial v_n}{\partial s} & \frac{1}{1-N}\frac{\partial v_z}{\partial s} \\ \frac{\partial v_s}{\partial n} & \frac{\partial v_n}{\partial n} & \frac{\partial v_z}{\partial n} \\ \frac{\partial v_s}{\partial z} & \frac{\partial v_n}{\partial z} & \frac{\partial v_z}{\partial z} \end{bmatrix} \tag{9}$$

in which r_c is the radius of curvature of the river centerline and $N = n/r_c$ a scale factor. The derivation of equation 9 is given in Appendix II. The complete determination of equation 7 is rather complex. Fortunately not all components of this equation are equally important. If only

the situation of a moderately meandering, shallow river with steady, subcritical flow is considered, several components can be neglected. First, because of the assumption of incompressible fluid, the contribution of the normal stresses τ_{ss}, τ_{nn} and τ_{zz} can be neglected. In addition, moderate meandering implicates small values of $\partial v_s / \partial n$ and $\partial v_n / \partial s$ making τ_{sn} and τ_{ns} small compared to τ_{sz} and τ_{nz}. The contribution of these components to the solution is thought to be at least an order of magnitude less than the contribution of the other components, so the error introduced by neglecting these components in relatively small. Finally in a shallow river, flow near the banks is small and relatively unimportant, so when bankflow is neglected, the gradients of vertical velocity $\partial v_z / \partial s$ and $\partial v_z / \partial n$ can also be neglected. Therefore the effective width of a river (w_e) is introduced as the part of the river not influenced by bankflow (see Figure 7). After these simplifications, calculation of the tensor product (equation 7) results in an expression for σ only dependent on the vertical gradients of the longitudinal and transverse velocity (Van Andel, 2002). Because the main interest is in the distribution of the entropy production along the river, this expression is integrated over a cross section of the river. This yields:

$$\sigma_{cs} = \frac{\rho}{T} \int_{-\frac{1}{2}w_e}^{\frac{1}{2}w_e} \int_{0}^{d} \varepsilon \left(\left(\frac{\partial v_s}{\partial z} \right)^2 + \left(\frac{\partial v_n}{\partial z} \right)^2 \right) dz dn \qquad (10)$$

in which σ_{cs} is the entropy production for a cross-section of a river or per unit length, w_e is the effective river width and d is the local depth. In order to quantify equation 10 the distribution of the longitudinal and transverse velocities in a meander bend have to be known. The flow model used to calculate these velocities is described in Section IV. With the assumption of steady flow it is implied that the meander planform is determined by one unique discharge. This assumption is also used by Chang (1979, 1984), Ikeda et al. (1981), Parker et al. (1982, 1983), Odgaard (1986*a*, 1986*b*) and many others. Usually the bankful discharge is taken as the unique discharge, which normally occurs once a year on average (Williams, 1978).

IV. Application of the Meander Flow Model

Model choice

In order to evaluate equation 9 along a meander bend, the velocity distributions have to be known. Therefore a model is needed that describes the (stationary) flow and bed topography in a meander bend. The Meander flow model developed by Odgaard (1986*a*) is employed here. The most important reason for choosing this model is that it is based on the same assumptions as made in Section III. The model applies to steady, subcritical, turbulent flow in shallow, moderately meandering rivers of relatively constant width and with uniform bed sediment. Furthermore, as in the derivation of equation 10, bankflow is neglected. The constraints are (Odgaard, 1986*a*): (1) effective river width is constant; (2) centerline radius of curvature is large compared with width; (3) large width/depth ratio; (4) transverse velocity components are small compared to longitudinal; (5) the turbulence is isotropic. Fortunately, these constraints are not in contradiction with the goal of finding the most probable shape of a regular meander under ideal circumstances. Another advantage of the model is its simplicity. This makes it less difficult to interpret the results. In this section only a brief summary of the model will be given. A more complete description can be found in Appendix III or in Odgaard (1986*a*).

Because it was shown that meandering is not dependent of scale it is convenient to have the model also independent of scale. The Meander flow model is slightly modified for a dimensionless treatment. The dimensions present in the problem are length, time, mass and temperature. Since the entropy production in equation 14 will be written times temperature and per unit mass, only characteristic scales for length and time have to be defined. For both quantities a suitable reference value is present in the model. Both effective width and centerline depth are assumed constant in the model, as well as the averaged centerline longitudinal velocity. Therefore all lengths are normalized with respect to width and all velocities are normalized with respect to the averaged centerline longitudinal velocity. As an example, the dimensionless downstream direction $\tilde{s}$ and transverse velocity $\tilde{v}_n$ can be written as:

$$\tilde{s} = \frac{s}{w_e}, \quad s = \tilde{s} w_e \qquad (11a)$$

$$\tilde{v}_n = \frac{v_n}{\overline{v}_{sc}}, \quad v_n = \tilde{v}_n \overline{v}_{sc} \qquad (11b)$$

in which the tilde denotes a dimensionless variable. The characteristic time scale results from combining equations 11a and 11b. Because the bed topography and the longitudinal velocity profile are dependent on the actual velocity and friction coefficient (which are not determined in a dimensionless treatment), a fully dimensionless treatment is not possible. However the scale dependent parameters are found to have only small effect on the results (see Section V).

Velocity profiles and calculation of entropy production

First a description is given of the velocity profiles in the Meander flow model. Because these profiles are given by simple analytical relationships it is possible to solve the first integral of equation 10. This results in an expression of σ_{cs} no longer directly dependent on vertical changes in velocity. The general power law is used to describe the vertical distribution of the longitudinal velocity (Odgaard, 1986a, his equation 3):

$$\frac{\tilde{v}_s}{\bar{\tilde{v}}_s} = \frac{m+1}{m}\left(\frac{\tilde{z}}{\tilde{d}}\right)^{\frac{1}{m}} \tag{12}$$

in which the dimensionless velocity-profile exponent m is a linear function of the Chezy coefficient. The vertical transverse velocity profile is assumed to be linear. Because the mass-shift, assumed in the Odgaard (1986*a*), model has no influence on the shape of the velocity profile, neglecting the mass shift leads to the relationship (Odgaard, 1986a, his equation 4):

$$\frac{\tilde{v}_n}{\tilde{v}_{ns}} = 2\left(\frac{\tilde{z}}{\tilde{d}} - \frac{1}{2}\right) \tag{13}$$

in which $\tilde{v}_{ns}$ is the transverse surface velocity. Again the interaction with the riverbed is not accounted for. Therefore the violation of the no-slip condition on the riverbed is legitimate. Examples of the velocity profiles described by equations 12 and 13 are given in Figure 7.

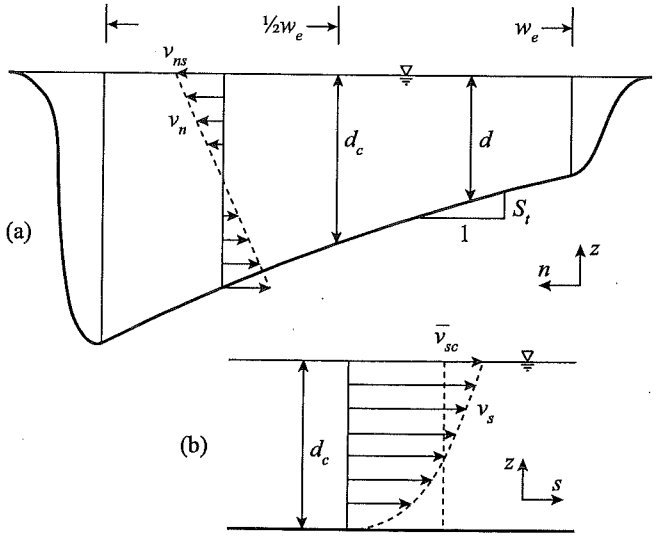

Figure 7. Longitudinal and transverse vertical velocity profiles, transverse depth distribution and definition of model parameters.

With equations 12 and 13, it is possible to solve the first integral of equation 10. Normalizing σ_{cs} by the temperature, density, effective width and averaged centerline longitudinal velocity, integrating and rearranging of terms yields (see Appendix IV):

$$\tilde{\sigma}_{cs} = \frac{T\sigma_{cs}w_e}{\rho\bar{v}_{sc}^{\,3}} = \kappa^2 \int_{-\frac{1}{2}}^{\frac{1}{2}} \left(\frac{(m+1)^2}{4m^3+2m^4}\bar{\tilde{v}}_s^{\,3} + \frac{4\bar{\tilde{v}}_s\tilde{v}_{ns}^{\,2}}{6m} \right) d\tilde{n} \tag{14}$$

The entropy production is now only dependent on the transverse surface velocity and the averaged centerline longitudinal velocity. No further analytical solution is possible because no simple relationships exist between $\tilde{n}$ and the depth (which determines the magnitude of $\tilde{v}_{ns}$ and $\bar{\tilde{v}}_s$). Therefore the model will be solved numerically to determine these variables in the $\tilde{s},\tilde{n}$-plane. A complicated determination of the three-dimensional velocity field is thus avoided.

Model description and solution strategy

The starting point of the Meander flow model is the equation that describes the longitudinal or streamwise variation of the centerline transverse bedslope (S_{Tc}). This equation is derived from a combination of the equation of motion for the transverse velocity component, a parabolic eddy viscosity profile, a parabolic velocity profile, the mass balance at the centerline to compensate for mass-shift and a simple linear relationship between the transverse bedslope and the transverse velocity at the bottom. At the centerline of the river this yields (Odgaard, 1986a, his equation 30):

$$\frac{d^2S_{Tc}}{d\tilde{s}^2} + a'\frac{dS_{Tc}}{d\tilde{s}} + b'S_{Tc} = \frac{c'}{\tilde{r}_c} \tag{15}$$

in which a', b' and c' are functions depending on sediment characteristics and cross section geometry. In equation 15, only the centerline radius of curvature $\tilde{r}_c$ is a function of $\tilde{s}$. From the centerline transverse bedslope, the local transverse depth distribution can be calculated from the simple relationship (Odgaard, 1986a, his equation 48):

$$S_T = S_{Tc}\frac{\tilde{d}}{\tilde{d}_c}\frac{\tilde{r}_c}{\tilde{r}} \tag{16}$$

in which d_c is the (constant) centerline depth and $\tilde{r}$ is the local radius of curvature. The convex transverse depth distribution described by equation 16 is shown in Figure 7. The depth distribution is needed to calculate the longitudinal velocity distribution. From the equation of motion in longitudinal direction, written in terms of the average longitudinal velocity and with the use of the parabolic eddy viscosity profile, it follows that the change in average longitudinal velocity along a path of constant distance from the centerline can be approximately written as (Odgaard, 1986a, his equation 15):

$$\frac{d\bar{\tilde{v}}_s^{\,2}}{d\tilde{s}} + g'\frac{\tilde{d}_c}{\tilde{d}}\bar{\tilde{v}}_s^{\,2} = g'\frac{\tilde{r}_c}{\tilde{r}} \tag{17}$$

in which the function g' is again depending on sediment characteristics and cross section geometry. Finally it is assumed that the local transverse bedslope is proportional to the transverse bottom velocity. Since it follows from equation 13 that the transverse surface velocity has the same absolute value (but different sign) as the transverse bottom velocity, the transverse surface velocity can be written in terms of the centerline transverse bedslope as (Odgaard, 1986a, his equations 21 and 48):

$$\tilde{v}_{ns} = f'S_{Tc}\frac{\tilde{d}}{\tilde{d}_c}\frac{\tilde{r}_c}{\tilde{r}} \tag{18}$$

in which the function f' depends on sediment and flow characteristics and cross section geometry. The calculation process is summarized in Figure 8. First the centerline transverse bedslope is determined for one meander wavelength by solving the homogenous second order differential equation given by Equation 15 for the initial condition $S_{Tc}(0)=0$. With $S_{Tc}(s)$ the depth distribution is determined and the distribution of the averaged longitudinal velocity is determined by solving Equation 17 with the initial condition $\bar{v}_s(0,n)=1$. Finally the distribution of the transverse surface velocity is determined. With $\bar{v}_s(s,n)$ and $\tilde{v}_{ns}(s,n)$ the entropy production for each cross section can be determined (Equation 14). To avoid errors introduced by choosing initial conditions, the entropy production for complete meander bend $\tilde{\sigma}_{tot}$ is determined. As long as the value of $\tilde{\sigma}_{tot}$ is not constant, the complete calculation process is repeated with new initial conditions. The computational s,n-space (see Figure 6) is discreted into steps of 0.1w. The source code of the flow model (MEANDERMODEL) is given in Appendix VI.

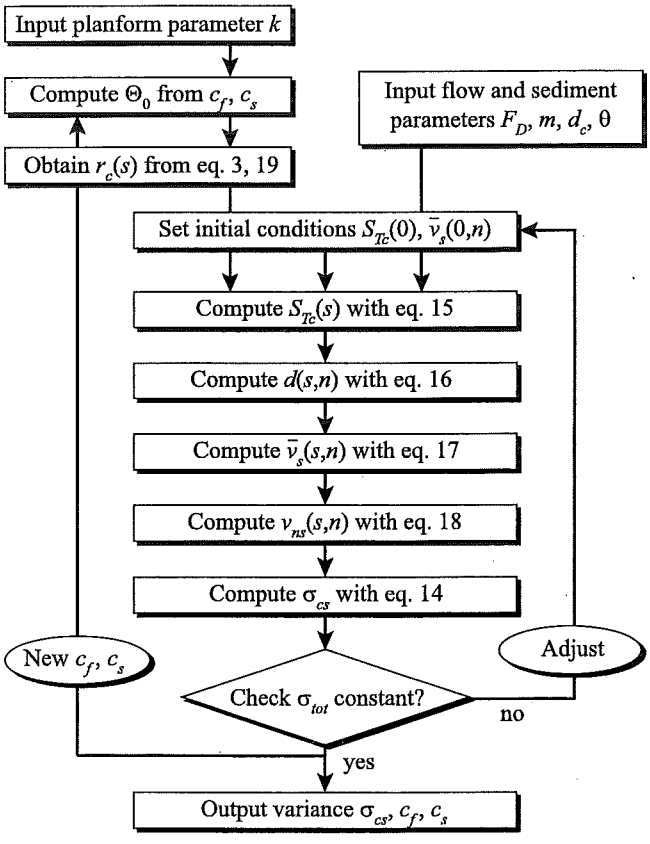

Figure 8. Flow chart of the calculation process (modified after Van Andel, 2002).

Scenarios

The main goal of the model study is to determine which meander planform results in the least variance of entropy production along a meander bend. Therefore the centerline radius of curvature as a function of the downstream location has to be known in the right hand side of equation 15. As a boundary condition to ease the interpretation of the results it is also demanded that a change in shape of the meander bend does not lead to a change in the meanderlength and wavelength. A formula that suits these conditions is given by the third order sine-generated curve (equation 3). From this equation, the longitudinal variation in the centerline radius of curvature is calculated by:

$$\frac{1}{\tilde{r}_c}=\frac{d\Theta}{d\tilde{s}} \tag{19}$$

There were several reasons for choosing the class of third order sine-generated curves as a description of the meander planform. First, the third order curves result from a theoretical analysis of flow and erosional processes in meander bends, and are nowadays widely accepted as a good description of meander planform. Furthermore with varying the fattening and skewing parameters a wide range of curves can be produced (Figure 4). For a given sinuosity this only leaves a clear and easy to handle two degrees of freedom. Finally, no fattening and skewing results in the "first order" sine-generated curve, the minimum variance curve when flow processes are not taken into account. The values of c_f and c_s are taken between –0.1 and 0.1, with intervals of 0.01. Higher or lower values result in unlikely curves. For each combination of these parameters Θ_0 is determined for a given sinuosity (see Determineparameters script in Appendix V). Each resulting curve is used as input of the Meander flow model (see Figure 8).

Since the Meander flow model is made dimensionless, the number of parameters that influences the result is strongly reduced. The spatial dimensions are all expressed in respect to the effective width, so only three spatial ratios remain to be chosen: the ratios of wavelength, meanderlength and depth to effective width. Since the empirical relation between width and wavelength was shown by Davy and Davies (1979) to be almost a fundamental relation and the power is very close to unity, the wavelength is assumed to equal eleven times the width:

$$\lambda=11.0w \tag{20}$$

With a constant wavelength, the meanderlength is determined by the sinuosity. Based on the work of Stølum (1996, 1998) a most probable sinuosity of π is assumed, corresponding to moderately meandering rivers. In natural rivers, all possible values of sinuosity can be found. It has been shown by Schumm et al. (1972) and Nagakawa and Scott (1984) that sinuosity is mainly determined by valley slope. As there is large variation in valley slopes, the influence of the sinuosity is investigated. A sinuosity of 5 is taken as maximum. Above this value cutoff's are likely to occur and the self-organized nature of this process (Stølum, 1996) indicates that this process is no longer determined by an increase in entropy. The depth/width ratio also shows considerable variations in natural rivers. A reference value of 0.1 is chosen, but the influence of this variable is also investigated. According to Odgaard (1986*a*)

bankflow influences the flow pattern to a distance of approximately one time the depth. With a depth/width ratio of 0.1, neglecting bankflow thus leads to a ratio of the wavelength to effective width of 13.2.

Besides the geometrical parameters mentioned above also two parameters related to flow and sediment characteristics are dependent on scale. Although the velocity profile exponent and the particle Froude number are both dimensionless, their value cannot be determined because the velocity profile exponent is a function of the scale dependent Chezy coefficient and the particle Froude number is a function of the actual velocity and sediment size (see Appendix IV). The values of the velocity profile exponent and the particle Froude number are taken as 2.8 respectively 6.78, the average values of the two river sites tested in Odgaard (1986*b*). On both parameters a sensitivity test is performed.

V. Results

The variance of the entropy production per cross section (equation 14) for different third order sine-generated meander curves with a constant sinuosity, clearly shows one unique minimum. This is shown in Figure 9, where the variance of σ_{cs} is plotted in the c_f, c_s-plane. From this figure it can be concluded that there is one "most probable" meander planform. The location of the minimum clearly differs from the first order sine-generated curve (located at (0,0)), which would result if the entropy production would be a simple linear function of the curvature. Linear interpolation shows that the minimum is located at (0.020,0.011). This leads to a fattening and upvalley skew in comparison with the first order sine-generated curve.

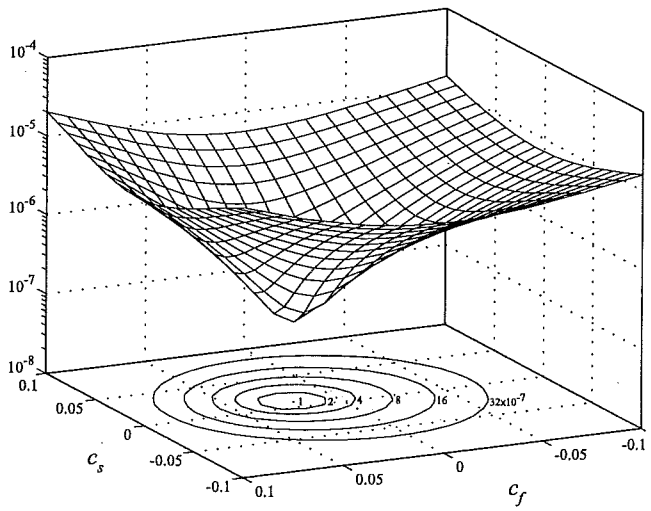

Figure 9. Variance of the entropy production per cross-section (vertical axis) versus fattening and skewing.

When the variance of the entropy production per cross section is interpreted as a measure of the probability, it can be seen from Figure 9 that the most probable meander planforms are found in the second quadrant. When compared with the first order sine-generated curve, fattening is more pronounced than skewing. This means that meanders with a negative fattening are unlikely to be found in nature. Since skewing is less pronounced, symmetric meanders or meanders with a slight downvalley skew should also occur in nature, but in smaller numbers. The probability of different types of third order sine-generated curves is discussed in more detail in Van Andel (2002).

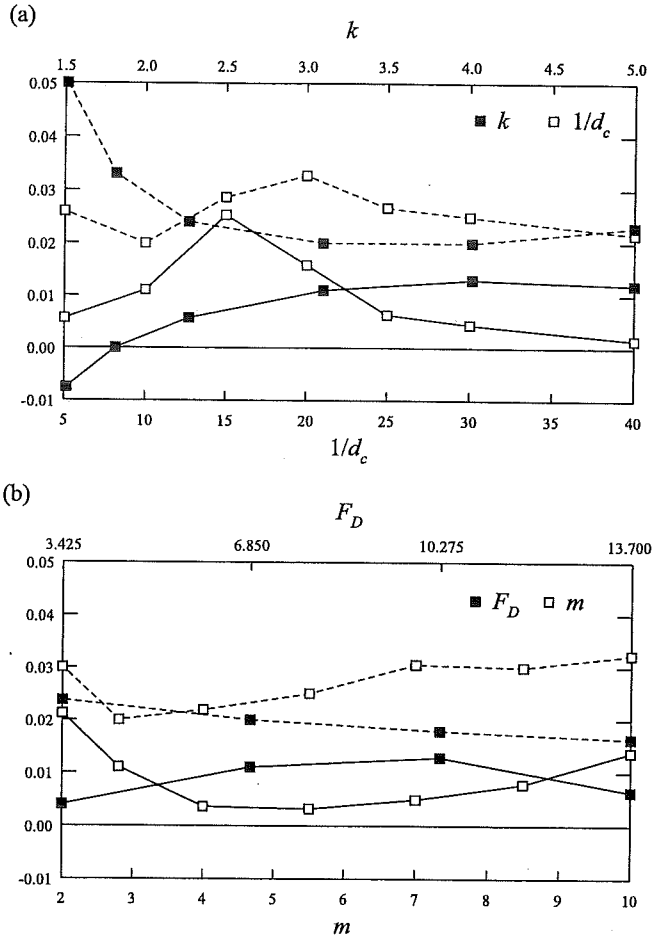

Figure 10. Effect of model parameters on the values of fattening (dotted line) and skewing (solid line). (a) Geometric parameters, (b) Flow and sediment parameters.

The results are dependent on two geometrical parameters and two parameters in the meander flow model, as discussed earlier. The effect of the sinuosity and the depth/width ratio on the result is shown in Figure 10a. The upvalley skew in meanders is the most pronounced at higher sinuosity's. At a sinuosity of 1.8, the model predicts a symmetric meander as the most probable one, while at an even lower sinuosity the most probable meander shows a slight downvalley skew. The less pronounced asymmetry at lower sinuosity's can also be seen from Figure 2. The influence of the sinuosity on the most probable meander planform is illustrated in Figure 11. The depth of the river also influences the most probable combination of fattening and skewing parameters. From Figure 10a it can be seen that there's a maximum upvalley skew at a depth of 1/15

times the effective width. The effect of the particle Froude number and the velocity profile exponent on the result is shown in Figure 10b. The particle Froude number (or flow regime) shows to have only little effect on the result. Skewing is more pronounced at low and high values of the velocity profile exponent, while at median values skewing is less pronounced.

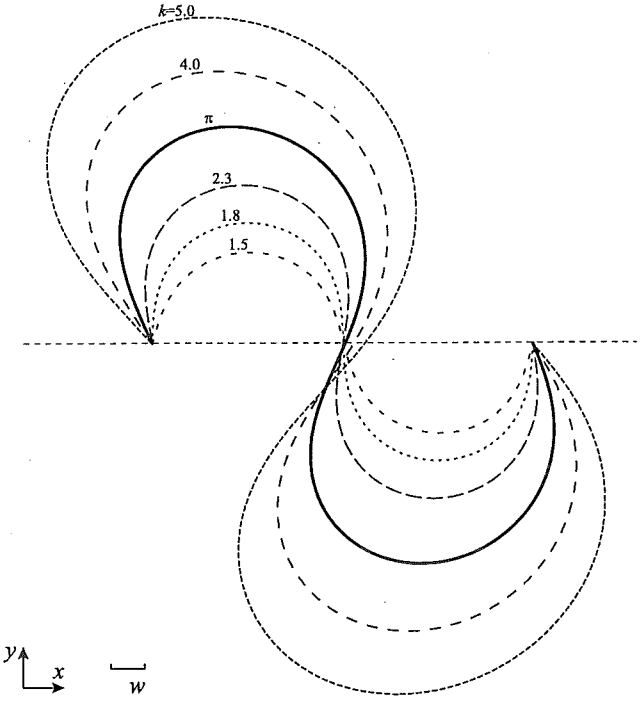

Figure 11. The most probable meander planform for different sinuosity's. Direction of flow is from left to right.

VI. Discussion

After seeing Figure 11, the most logical question is does the most probable meander planform predicted by the Meander flow model correspond to meanders found in nature? The answer to this question is much more complicated than the question itself. As a full comparison with natural meanders is beyond the aim of this study, only a brief comparison with one of the most famous meanders will be given. The meanders in the Mississippi River at Greenville (Miss., USA, see also Figure 2) have been used in previous studies on meandering to illustrate earlier attempts to explain the typical meander planform (Langbein and Leopold, 1966, Parker et al., 1983). Because the meanders in the Mississippi are very old and distinct, they can be assumed close to equilibrium and thus close to the curves presented in Figure 11. One complete wavelength of the Mississippi meanders is shown in Figure 12 and compared with the most probable third order sine-generated curve with the same sinuosity. Although not perfect, the similarity can be called convincing.

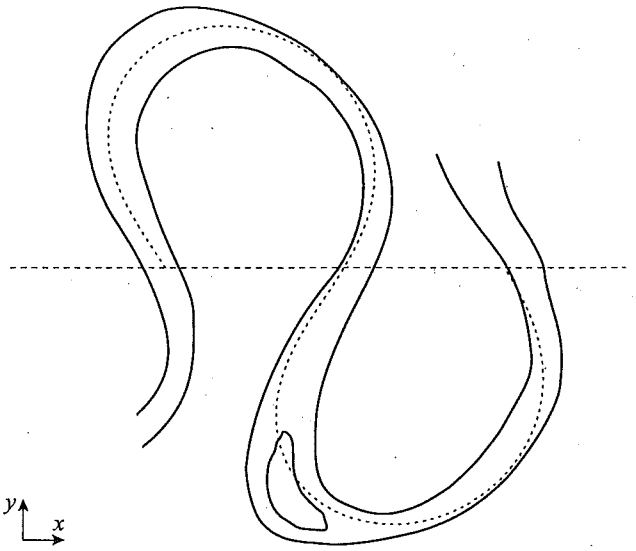

Figure 12. Mississippi River at Greenville, Miss., USA, before the artificial cutoffs (redrawn after Langbein and Leopold, 1966) compared with the third order sine-generated curves as predicted by maximum entropy principle. Direction of flow is from left to right.

Natural meanders often differ from the meanders drawn in Figure 11. The reason for this difference can be ascribed to the discrepancy between "ideal" regularly and stationary meanders and natural river meanders. In reality, a meander bend cannot be seen separated from the meandering river it is part of. And although the river system may continuously develop towards an increase in entropy, equilibrium is never reached because of constantly changing boundary conditions in natural rivers. These are the result of the occurrence of cut-off's as well as changes in flow regime. Furthermore irregularities in geology, sediment distribution, topography or other factors can prevent a river from developing towards maximum entropy. It can thus be assumed that only old and well-developed meanders are close to the most probable state (Langbein and Leopold, 1966) or the "ideal state" (Parker et al., 1983).

How can it be seen that the distribution of entropy production is indeed the parameter that determines the channel planform? One might instinctively suspect that it is not the distribution of the internal stress but the bed shear stress that determines the planform, as sediment transport and erosion are related to bed shear rather than internal shear in the fluid. But as laboratory measurements by Hooke (1975) showed, the distribution of sediment transport and bed shear in a meander bend is not evenly distributed, not even over a cross-section. From equation 10 it can be seen that the entropy production is only related to velocity gradients. Thus in a steady state the velocity gradients will also reflect a balanced situation with velocity gradients at the bed - which determine the complex pattern of local erosion and deposition. But as meandering is not restricted to the presence of sediment and the most probable state of a river is one with small sediment load, the

determination of this complex relation is of little importance in this study.

The round meander bends found in this study are partially in contradiction with the conclusions reached by Parker et al. (1983), who predicted a negative fattening leading to a sharper bend. However the more rounded asymmetrical bend resulting from positive fattening is similar to the meander bends drawn by Davis (1899, his Figure 50). The upvalley skew predicted in this study is in agreement with the conclusions reached by Carson and Lapointe (1983), who found that both types of asymmetry are found in nature, but that meanders with an upvalley skew have a greater probability. In Figure 13, the maximum entropy curve resulting from this study is compared with the curves predicted by the Theory of minimum variance (Langbein and Leopold, 1966) and the Bend equation (Parker et al., 1983). The difference in shape between the maximum entropy curve and the first order sine generated curve can be explained by the more conceptual rather than theoretical basis of the latter (see Section II). However to find an explanation for the difference in shape between the maximum entropy curve predicted by this study and the curve resulting from the Bend equation is much more difficult, as this difference is the result of a fundamentally different approach. Both curves share the same upvalley skewing, but the relatively sharp bends and long almost straight reaches between the bends in comparison with the rounded maximum entropy curve seem in contradiction with the curves found in nature (Figures 1, 2 and 5). An extensive study on the shape of and flow processes in meandering rivers is needed to provide data necessary to evaluate the results of the present study as well as past studies. Further study by means of easy controllable and small-scale surface tension meanders might be a useful in this respect.

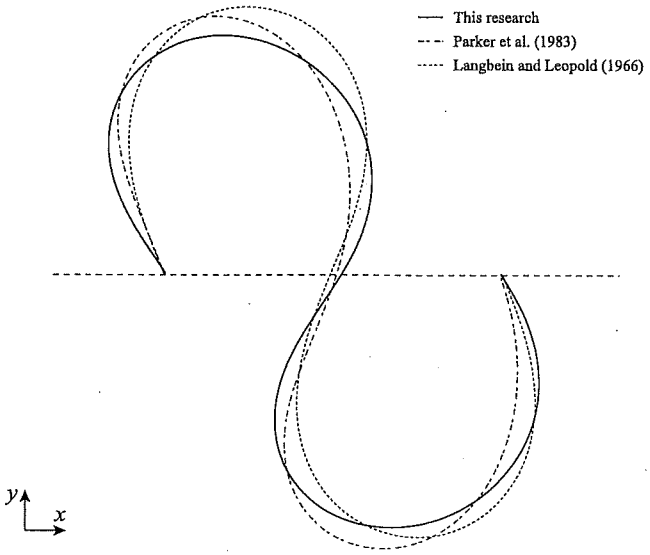

Figure 13. Comparison of the maximum entropy meander curve with the curves predicted by the Theory of minimum variance (Langbein and Leopold, 1966) and the bend equation (Parker et al., 1983). Direction of flow is from left to right.

Another question is how far the results are dependent on the methods that have been used. This is especially true for the choices of the flow model and the class of third order sine-generated curves. Although the results of the Meander flow model seem to agree well with field measurements, it is however possible that a model based on different assumptions will yield different results. The choice for the class of third order sine-generated curves was done by practical lack of alternatives. Although the curves seem able to describe natural meanders, they do not describe delayed inflection as found by Carson and Lapointe (1983). It might thus still be possible to find a meander planform resulting in an even lower variance of the entropy production. Using natural meander planforms as an input for the Meander flow model might be an important next step in this research.

VII. Conclusion

Although there have been numerous efforts to find an explanation of the typical meander planform, so far no general principle has been found that sufficiently explains the typical meander planform. In this study it was shown that the typical meander planform is the result of the thermodynamic principle of maximum entropy. The most probable distribution of the production of entropy along a meander bend is one in which the production of entropy is as low and as uniform as possible. This corresponds to a state of maximum entropy. For the methods used, the variance of the entropy production along a meander bend showed to be minimum for a slightly fattened and skewed curve when compared with the first order sine-generated curve suggested by Langbein and Leopold (1966). Their Theory of minimum variance thus showed to be inherent with meander asymmetry as documented by Carson and Lapointe (1983).

Acknowledgements

I would like to thank Peter Troch for supervising this research and for infecting me with the "meander"-virus, Schalk-Jan van Andel for his work and ideas that formed a major input for this paper, and Paul Torfs, Marc Hoffmann and C. Paniconi for critically reviewing this paper.

REFERENCES

Andel, S.J. van, 2002. Uniform energy dissipation explaining typical planform of river meander bend, MSc thesis, Wageningen University.

Berg, J.H. van den, 1995. Prediction of alluvial channel pattern of perennial rivers, *Geomorphology*, 12: 259-279.

Bird, R.B., W.E. Steward, and E.N. Lightfoot, 1960. Transport phenomena, Wiley, New York.

Brice, J.C., 1974. Evolution of meander loops, *Geol. Soc. America Bull.*, 85: 581-586.

Carson, M.A., and M.F. Lapointe, 1983. The inherent asymmetry of river meander planform, *J. Geol.*, 91: 41-55.

Chang, H.H., 1979. Minimum stream power and river channel patterns, *J. Hydrol.*, 41: 303-327.

Chang, H.H., 1984. Analysis of river meanders, *J. Hydraul. Engrg.*, ASCE, 110(1): 37-50.

Chitale, S.V., 1973. Theories and relationships of river channel patterns, *J. Hydrol.*, 19: 285-308.

Crosato, A., 1990. Simulation of meandering river processes, *Comm. on Hydraul. and Geotech. Engrg.*, Delft Univ. of Technol., 90(3).

Davis, W.M., 1899. The geographical cycle, Geographical Journal, XIV, 481-504. Reprinted in: Davis, W.M., 1954. Geographical essays, Dover Publ., 777 p.

Davies, T.R.H., and C.C. Tinker, 1984. Fundamental characteristics of stream meanders, *Geol. Soc. America Bull.*, 95: 505-512.

Davy, B.W., and T.R.H. Davies, 1979. Entropy concepts in fluvial geomorphology: a reevaluation, *Wat. Resour. Res.*, 15(1): 103-106.

Denbigh, K.G., 1951. The thermodynamics of the steady state, Methuen & Co., London, 86 p.

Dozier, J., 1976. An examination of the variance minimization tendencies of a supraglacial stream, *J. Hydrol.*, 31: 359-380.

Einstein, A., 1926. The cause of the formation of meanders in the courses of rivers and the so-called Baer's law, in: Einstein A centenary volume, Heinemann, London, 1979.

Ferguson, R.I., 1973. Sinuosity of supraglacial streams, *Geol. Soc. America Bull.*, 84: 251-256.

Flamant, A., 1891. Hydraulique, Ponts et chaussées, Paris, 685 p.

Harris, J.W., and H. Stocker, 1998. Handbook of mathematical and computational science, Springer, New York, 1028 p.

Hey, R.D., 1976. Geometry of river meanders, *Nature*, 262: 482-484.

Hooke, R. le B., 1975. Distribution of sediment transport and shear stress in a meander bend, *J. Geol.*, 83(5): 543-565.

Howard, A.D., and T.R. Knutson, 1984. Sufficient conditions for river meandering: a simulation approach, *Water Resour. Res.*, 20(11): 1659-1667.

Huang, H. Q., and G.C. Nanson, 2000. Hydraulic geometry and maximum flow efficiency as products of the principle of least action, *Earth Surf. Proc. and Landf.*, 25: 1-16.

Ikeda, M., J.A. Johannessen, K. Lygre, S. Sandven, 1989. A process study of mesoscale meanders and eddies in the Norwegian coastal current. *J. Phys. Oceanography*, 19(1): 20–35.

Ikeda, S., G. Parker, and K. Sawai, 1981. Bend theory of river meanders. Part 1. Linear development, *J. Fluid Mech.*, 112: 363-377.

Jefferson, M.S.W., 1902. The limiting width of meander belts, *National. Geogr. Mag.*, Oct., 373-384.

Jennings, J.N., 1972. Karst, M.I.T. Press, Massachusetts, 253 p.

Komatsu, V., and V.R. Baker, 1994. Meander properties of Venusian channels, Geology, 22: 67-70.

Lancaster, S.T., and R.L. Bras, 2002. A simple model of river meandering and its comparison to natural channels, *Hydrol. Processes*, 16: 1-26.

Langbein, W.B., and L.B. Leopold, 1966. River meanders - theory of minimum variance, *U.S. Geol. Surv. Prof. Pap.*, 422-H.

Leopold, L.B., 1995. A view of the river, Hardvard Univ. Press, London, 298 p.

Leopold, L.B., and W.B. Langbein, 1962. The concept of entropy in landscape evolution, *U.S. Geol. Surv. Prof. Pap.*, 500-A.

Leopold, L.B., and W.B. Langbein, 1966. River meanders, *Sci. Am.*, 214(June): 60-70.

Lewin, J., and P.A. Brewer, 2001. Predicting channel patterns, *Geomorphology*, 40: 329-339.

Lord Kelvin, 1876. On the winding of rivers in alluvial plains, *Proc. Royal Soc. London*, A25, 5-8.

Meakin, P., T. Sun, T. Jøssang, and K. Schwarz, 1996. A simulation model for meandering rivers and their associated sedimentary environments, *Physica A*, 233: 606-618.

Mizumura, K., 1993. Meandering water rivulet, *J. Hydraul. Engrg.*, 119(11): 1205-1222.

Mizumura, K., and M. Yamasaka, 1997. Analysis of meandering water rivulets of finite amplitude, *J. Hydraul. Engrg.*, ASCE, 123(11): 995-1003.

Molnár, P., and J.A. Ramírez, 1998. Energy dissipation theories and optimal channel characteristics of river networks, *Wat. Resour. Res.*, 34(7): 1809-1818.

Morse, P.H., and H. Feshbach, 1953. Methods of theoretical physics, McGraw-Hill, New York, 1978 p.

Nakagawa, T., and J.C. Scott, 1984. Stream meanders on a smooth hydrophobic surface, *J. Fluid Mech.*, 149: 89-99.

Odgaard, A.J., 1986*a*. Meander flow model. I: Development, *J. Hydraul. Engrg.*, ASCE, 112(12): 1117-1136.

Odgaard, A.J., 1986*b*. Meander flow model. II: Applications, *J. Hydraul. Engrg.*, ASCE, 112(12): 1137-1150.

Ohanian, H.C., 1989. Physics, W.W. Norton, New York, 1148 p.

Parker, G., P. Diplas, and J. Akiyama, 1983. Meander bends of high amplitude, *J. Hydraul. Engrg.*, ASCE, 109(10): 1323-1337.

Parker, G., K. Sawai, and S. Ikeda, 1982. Bend theory of river meanders. Part 2. Nonlinear deformation of finite-amplitude bends, *J. Fluid Mech.*, 115: 303-314.

Prigogine, I., and I. Stengers, 1985. Order out of chaos: man's new dialogue with nature, Fontana, London, 349 p.

Schumm, S.A., H.R. Khan, B.R. Winkeley and L.G. Robbins, 1972. Variability of river patterns, *Nature Phys. Sci.*, 237: 75-76.

Smith, C.E., 1998. Modeling high sinuosity meanders in a small flume, *Geomorphology*, 25: 19-30.

Smith, J.D., and S.R. McLean, 1984. A model for flow in meandering streams, *Water Resour. Res.*, 20(9): 1301-1315.

Song, C.C.S., 1992. The role of energy dissipation in fluid flows and river mechanics. In: Singh, V.P., and Fiorentino, M. (ed.), Entropy and energy dissipation in water resources, Kluwer, Dordrecht.

Stølum, H.H., 1996. River meandering as a self-organization process, *Science*, 271: 1710-1714.

Stølum, H.H., 1998. Planform geometry and dynamics of meandering rivers, *Geol. Soc. America Bull.*, 110: 1485-1498.

Sun, T., P. Meakin, and T. Jøssang, 1996. A simulation model for meandering rivers, *Water Resour. Res.*, 32(9): 2937-2954.

Sun, T., P. Meakin, and T. Jøssang, 2001a. A computer model for meandering rivers with multiple bed load sediment sizes; 1. Theory, *Water Resour. Res.*, 37(8): 2227-2241.

Sun, T., P. Meakin, and T. Jøssang, 2001b. A computer model for meandering rivers with multiple bed load sediment sizes; 2. Computer simulations, *Water Resour. Res.*, 37(8): 2243-2258.

Thorne, C.R., and R.D. Hey, 1979. Direct measurements of secondary currents at a river inflexion point, *Nature*, 280: 226-228.

Williams, G.P., 1978. Bank-full discharge of rivers, *Water Resour. Res.*, 14(6): 1141-1154.

Woldenberg, M.J., 1966. Horton's laws justified in terms of allometric growth and steady state in open systems, *Geol. Soc. America Bull.*, 77: 431-434.

Yang, C.T., 1971. On river meanders, *J. Hydrol.*, 13: 231-253.

Yang, C.T., 1992. Force, energy, entropy and energy dissipation rate. In: Singh, V.P., and Fiorentino, M. (ed.), Entropy and energy dissipation in water resources, Kluwer, Dordrecht.

Yang, C.T., and C.C.S. Song, 1979. Theory of minimum rate of energy dissipation, *J. Hydraul. Div.*, ASCE, 105(7): 769-784.

APPENDIX I. DERIVATION OF EQUATION 7 FROM FIRST LAW OF THERMODYNAMICS

An expression for the entropy production can be derived by starting with the first law of thermodynamics, which states that the difference between the heat (Q) added to a system and the work (W) done by a system equals the increase of energy (E):

$$\Delta Q - \Delta W = dE \tag{AI-1}$$

For a fluid particle work is done by gravitational, pressure and viscous forces. The energy term in AI-1 includes both kinetic energy as well as internal energy. Written in terms of rate of change per unit mass for an infinitesimal volume, with ρ assumed constant, equation AI-1 can be written as (Bird et al., 1960, p. 313):

$$\rho \frac{D\left(\frac{1}{2}v^2 + e_i\right)}{Dt} = -(\nabla \cdot \boldsymbol{q}) + p(\boldsymbol{g} \cdot \boldsymbol{v}) - (\nabla \cdot p\boldsymbol{v}) - (\nabla \cdot [\boldsymbol{\tau} \cdot \boldsymbol{v}]) \tag{AI-2}$$

To obtain the equation for change of e_i, equation AI-2 is subtracted by the equation that gives the rate of change of kinetic energy per unit mass for an element of fluid moving downstream. This equation is obtained by multiplying the equation of motion with the local velocity v:

$$\rho \frac{D\left(\frac{1}{2}v^2\right)}{Dt} = p(\nabla \cdot \boldsymbol{v}) - (\nabla \cdot p\boldsymbol{v}) + \rho(\boldsymbol{v} \cdot \boldsymbol{g}) - (\boldsymbol{v} \cdot [\nabla \cdot \boldsymbol{\tau}]) \tag{AI-3}$$

With the vector identity $\boldsymbol{v} \cdot [\nabla \cdot \boldsymbol{\tau}] = \nabla \cdot [\boldsymbol{\tau} \cdot \boldsymbol{v}] - \boldsymbol{\tau} : \nabla \boldsymbol{v}$ (Bird et al., 1960, p. 731) subtraction of equation AI-3 from equation AI-2 yields the equation of the rate of change for the internal energy of a fluid particle:

$$\rho \frac{De_i}{Dt} = -(\nabla \cdot \boldsymbol{q}) - p(\nabla \cdot \boldsymbol{v}) - (\boldsymbol{\tau} : \nabla \boldsymbol{v}) \tag{AI-4}$$

For an isothermal system (no heat flow) and incompressible fluid the equation becomes:

$$\rho \frac{De_i}{Dt} = -(\boldsymbol{\tau} : \nabla \boldsymbol{v}) \tag{AI-5}$$

This equation describes the irreversible rate of internal energy increase per unit volume by viscous dissipation (potential energy is dissipated into heat). Because this process is irreversible, the right-hand side of equation AI-5 also describes the increase in disorder or entropy. With the substitution of $\rho De_i / Dt = T\sigma$, the equation thus becomes (Yang, 1992):

$$T\sigma = -(\boldsymbol{\tau} : \nabla \boldsymbol{v}) \tag{7}$$

where σ is the entropy production per unit volume and T is the absolute temperature.

APPENDIX II. COORDINATE TRANSFORMATION AND SIMPLIFICATION OF EQUATION 7.

In this appendix equation 7 will be rewritten in a right-handed, orthogonal, curvilinear coordinate system with a downstream s-axis, across-stream n-axis and a vertical z-axis. According to Bird et al. (1960, p. 739), the gradient vector in curvilinear coordinates can be written as:

$$\nabla = \sum_\alpha \frac{\delta_\alpha}{h_\alpha} \frac{\partial}{\partial q_\alpha} \tag{AII-1}$$

in which δ_α is the unit vector in direction q_α of the "new" coordinate system and h_α is a scale factor in the direction q_α. The scale factors h_α are determined by (Morse and Feshbach, 1953, p. 24):

$$h_\alpha^2 = \left(\frac{\partial x}{\partial q_\alpha}\right)^2 + \left(\frac{\partial y}{\partial q_\alpha}\right)^2 + \left(\frac{\partial z}{\partial q_\alpha}\right)^2 \tag{AII-2}$$

in which x, y and z are Cartesian coordinates. As illustrated in figure AII-1, the Cartesian coordinates can be related to the curvilinear coordinates by (Smith and McLean, 1984):

$$x = x_0 - \Delta x = x_0 - n\cos\beta = x_0 - n\frac{dy_0}{ds} \tag{AII-3a}$$

$$y = y_0 + \Delta y = y_0 + n\sin\beta = y_0 + n\frac{dx_0}{ds} \tag{AII-3b}$$

where the centreline of the river is given by the Cartesian coordinates (x_0, y_0) (fig. AII-1).

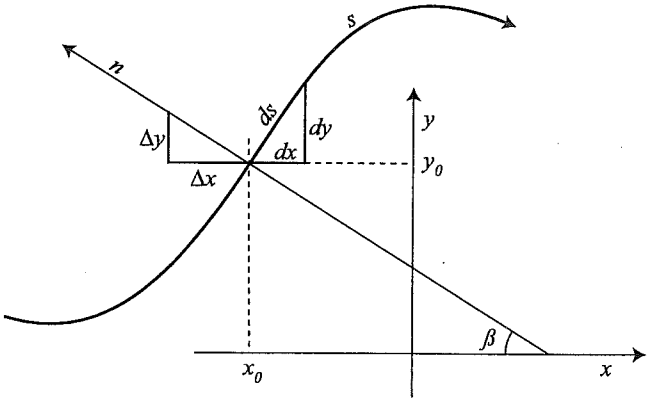

Figure AII-1. Definition sketch for the curvilinear coordinate system (after Smith and McLean, 1984).

The radius of curvature of the river centreline is given by (Harris and Stocker, 1998, p.520):

$$r_c(s) = \left(-\frac{d\beta}{ds}\right)^{-1} = \left(\frac{dx_0}{ds}\frac{d^2y_0}{ds^2} - \frac{d^2x_0}{ds^2}\frac{dy_0}{ds}\right)^{-1} \tag{AII-4}$$

With $q_1 = s$, $q_2 = n$ and $q_3 = z$, the scale factor h_1 is determined as follows:

$$\frac{dx}{ds}=\frac{dx_0}{ds}-n\frac{d^2y_0}{ds^2} \qquad \text{(AII-5a)}$$

$$\frac{dy}{ds}=\frac{dy_0}{ds}+n\frac{d^2x_0}{ds^2} \qquad \text{(AII-5b)}$$

$$\frac{dz}{ds}=0 \qquad \text{(AII-5c)}$$

so the equation for h_1 becomes:

$$h_1=\left(\left(\frac{dx_0}{ds}\right)^2+\left(\frac{dy_0}{ds}\right)^2+n^2\left(\left(\frac{d^2y_0}{ds^2}\right)^2+\left(\frac{d^2x_0}{ds^2}\right)^2\right)-2n\left(\frac{dx_0}{ds}\frac{d^2y_0}{ds^2}-\frac{dy_0}{ds}\frac{d^2x_0}{ds^2}\right)\right)^{\frac{1}{2}} \qquad \text{(AII-6)}$$

With the help of equations AII-4 and AII-5 this can be written as:

$$h_1=\left(1-\frac{2n}{r_c}+n^2\left(\frac{d\beta}{ds}\right)^2\right)^{\frac{1}{2}}=\left(1-\frac{2n}{r_c}+\frac{n^2}{r_c^2}\right)^{\frac{1}{2}}=1-N \qquad \text{(AII-7)}$$

in which $N=n/r_c$. The other scale factors h_2 and h_3 are unity. With these scale factors inserted in equation AII-1, the gradient vector in curvilinear coordinates becomes:

$$\nabla=\frac{\boldsymbol{\delta}_s}{1-N}\frac{\partial}{\partial s}+\boldsymbol{\delta}_n\frac{\partial}{\partial n}+\boldsymbol{\delta}_z\frac{\partial}{\partial z} \qquad \text{(AII-8)}$$

In order to calculate $\nabla\boldsymbol{v}$ in equation 7, it is convenient first to focus on the spatial derivatives of the unit vectors in curvilinear coordinates. These derivatives can be obtained according to (Bird et al., 1960, p. 739):

$$\frac{\partial\boldsymbol{\delta}_\alpha}{\partial q_\beta}=\frac{\boldsymbol{\delta}_\beta}{h_\alpha}\frac{\partial h_\beta}{\partial q_\alpha}-\delta_{\alpha\beta}\sum_{i=3}^{3}\frac{\boldsymbol{\delta}_i}{h_i}\frac{\partial h_\alpha}{\partial q_i} \qquad \text{(AII-9)}$$

in which $\delta_{\alpha\beta}$ is the Kronecker delta. The Kronecker delta can be written as:

$$\delta_{\alpha\beta}=\left(\boldsymbol{\delta}_\alpha\cdot\boldsymbol{\delta}_\beta\right) \qquad \text{(AII-10)}$$

It can be seen that the Kronecker delta is 1 for $\alpha=\beta$ and 0 for $\alpha\neq\beta$. This results in the following expressions for the spatial derivatives of the unit vectors:

$$\frac{\partial\boldsymbol{\delta}_s}{\partial s}=-\frac{\boldsymbol{\delta}_s}{1-N}\frac{\partial N}{\partial s}+\boldsymbol{\delta}_{ss}\left(\frac{\boldsymbol{\delta}_s}{1-N}\frac{\partial N}{\partial s}+\frac{\boldsymbol{\delta}_n}{r_c}\right)=\boldsymbol{\delta}_n\frac{1}{r_c} \qquad \text{(AII-11)}$$

$$\frac{\partial\boldsymbol{\delta}_n}{\partial s}=-\boldsymbol{\delta}_s\frac{1}{r_c} \qquad \text{(AII-12)}$$

All other expressions are equal to zero. The dyadic product $\nabla\boldsymbol{v}$ results in a tensor. The nine tensor components can be calculated according to:

$$\nabla\boldsymbol{v}=\left\{\frac{\boldsymbol{\delta}_s}{1-N}\frac{\partial}{\partial_s}+\boldsymbol{\delta}_n\frac{\partial}{\partial_n}+\boldsymbol{\delta}_z\frac{\partial}{\partial_z}\right\}\left\{\boldsymbol{\delta}_s v_s+\boldsymbol{\delta}_n v_n+\boldsymbol{\delta}_z v_z\right\} \qquad \text{(AII-13)}$$

As an example the first tensor component (corresponding to $\boldsymbol{\delta}_s\boldsymbol{\delta}_s$) is calculated below:

$$\frac{\boldsymbol{\delta}_s}{1-N}\frac{\partial}{\partial s}\left(\boldsymbol{\delta}_s v_s\right)=\frac{\boldsymbol{\delta}_s}{1-N}\left(v_s\left(\boldsymbol{\delta}_n\frac{1}{r_c}\right)+\boldsymbol{\delta}_s\frac{\partial v_s}{\partial s}\right)=\frac{\boldsymbol{\delta}_s\boldsymbol{\delta}_n}{r_c-n}v_s+\frac{\boldsymbol{\delta}_s\boldsymbol{\delta}_s}{1-N}\frac{\partial v_s}{\partial s} \qquad \text{(AII-14)}$$

Similarly, another part of the first component follows from:

$$\frac{\boldsymbol{\delta}_s}{1-N}\frac{\partial}{\partial s}\left(\boldsymbol{\delta}_n v_n\right)=\boldsymbol{\delta}_s\boldsymbol{\delta}_n\frac{1}{1-N}\frac{\partial v_n}{\partial s}-\boldsymbol{\delta}_s\boldsymbol{\delta}_s\frac{v_n}{r_c-n} \qquad \text{(AII-15)}$$

The first tensor component is given by summarizing all terms with $\boldsymbol{\delta}_s\boldsymbol{\delta}_s$:

$$\frac{1}{1-N}\frac{\partial v_s}{\partial s}-\frac{v_n}{r_c-n} \qquad \text{(AII-16)}$$

The complete dyadic product $\nabla\boldsymbol{v}$ can be written as follows:

$$\nabla v_{ij}=\begin{bmatrix}\frac{1}{1-N}\frac{\partial v_s}{\partial s}-\frac{v_n}{r_c-n} & \frac{v_s}{r_c-n}+\frac{1}{1-N}\frac{\partial v_n}{\partial s} & \frac{1}{1-N}\frac{\partial v_z}{\partial s}\\ \frac{\partial v_s}{\partial n} & \frac{\partial v_n}{\partial n} & \frac{\partial v_z}{\partial n}\\ \frac{\partial v_s}{\partial z} & \frac{\partial v_n}{\partial z} & \frac{\partial v_z}{\partial z}\end{bmatrix} \qquad (9)$$

With the expression for $\nabla\boldsymbol{v}$ in curvilinear coordinates, focus is now on the expression of the stress tensor $\boldsymbol{\tau}$ in velocity gradients. Because flow in rivers is almost always turbulent, transport of momentum will occur mainly by convection rather than by molecular motion, so Newton's law of viscosity for laminar flow cannot be used here. A solution was offered by the famous hydrologist Boussinesq in 1877, who introduced the kinematic eddy viscosity in analogy with the kinematic viscosity in laminar flow. The eddy viscosity is however not a property of the fluid but of the flow, and it can be used in systems where the diffusion of momentum is mainly in vertical direction and where the horizontal transfer of momentum is of little importance (Smith and McLean, 1984). If we assume that, in analogy with laminar flow, the stress tensor for turbulent flow can be written as the product of a scalar eddy viscosity ε and a rate of strain tensor $\boldsymbol{\psi}$, the components of the stress tensor are given by:

$$\tau_{ij} = -2\rho\varepsilon\psi_{ij} \tag{8a}$$

The rate of strain is given by:

$$\psi_{ij} = \frac{1}{2}\left(\nabla v_{ij} + \nabla v_{ji}\right) \tag{8b}$$

The components of the rate of strain tensor can be determined from equation 9. This results in the following six unique components of the stress tensor:

$$\tau_{ss} = -2\rho\varepsilon\left(\frac{1}{1-N}\frac{\partial v_s}{\partial s} - \frac{v_n}{r_c - n}\right) \tag{AII-17a}$$

$$\tau_{nn} = -2\rho\varepsilon\left(\frac{\partial v_n}{\partial n}\right) \tag{AII-17b}$$

$$\tau_{zz} = -2\rho\varepsilon\left(\frac{\partial v_z}{\partial z}\right) \tag{AII-17c}$$

$$\tau_{zs} = \tau_{sz} = -\rho\varepsilon\left(\frac{1}{1-N}\frac{\partial v_z}{\partial s} + \frac{\partial v_s}{\partial z}\right) \tag{AII-17d}$$

$$\tau_{zn} = \tau_{nz} = -\rho\varepsilon\left(\frac{\partial v_z}{\partial n} + \frac{\partial v_n}{\partial z}\right) \tag{AII-17e}$$

$$\tau_{ns} = \tau_{sn} = -\rho\varepsilon\left(\frac{1}{1-N}\frac{\partial v_n}{\partial s} + \frac{v_s}{r_c - n} + \frac{\partial v_s}{\partial n}\right) \tag{AII-17f}$$

The scalar product (also called double dot product) of the two tensors τ and ∇v can be calculated from (Bird et al., 1960, p.731):

$$\left(\boldsymbol{\tau} : \nabla \boldsymbol{v}\right) = \sum_i \sum_j \tau_{ij} \frac{\partial}{\partial q_j} v_i \tag{AII-18}$$

resulting in an expression with nine terms. Fortunately not all components of this equation are equally important. If only the situation of a moderately meandering, shallow river with steady, subcritical flow is considered, several components can be neglected. First, because of the assumption of incompressible fluid, the contribution of the normal stresses τ_{ss}, τ_{nn} and τ_{zz} can be neglected. In addition, moderately meandering implicates small values of $\partial v_s / \partial n$ and $\partial v_n / \partial s$ making τ_{sn} and τ_{ns} small compared to τ_{sz} and τ_{nz}. The contribution of these components to the solution is thought to be at least an order of magnitude less than the contribution of the other components, so the error introduced by neglecting these components in relatively small. Finally in a shallow river, flow near the banks is small and relatively unimportant, so when bankflow is neglected, the gradients of vertical velocity $\partial v_z / \partial s$ and $\partial v_z / \partial n$ can also be neglected. Therefore the effective width of a river (w_e) is introduced as the part of the river not influenced by bankflow (see Figure 6). After these simplifications, calculation of the tensor product (equation 7) results in an expression for σ only dependent on the vertical gradients of the longitudinal and transverse velocity (Van Andel, 2002):

$$\left(\boldsymbol{\tau} : \nabla \boldsymbol{v}\right) = -\rho\varepsilon\left(\frac{\partial v_s}{\partial z}\right)^2 - \rho\varepsilon\left(\frac{\partial v_n}{\partial z}\right)^2 \tag{AII-19}$$

or:

$$\sigma = \frac{\rho\varepsilon}{T}\left(\left(\frac{\partial v_s}{\partial z}\right)^2 + \left(\frac{\partial v_n}{\partial z}\right)^2\right) \tag{AII-20}$$

APPENDIX III. DESCRIPTION OF MEANDER FLOW MODEL

The model used here to calculate velocity profiles in a meander bend of arbitrary shape was developed by Odgaard (1986). It applies to steady, subcritical, turbulent flow in rivers with uniform bed sediment. Similar to the assumption made earlier in the derivation of the entropy production equation, bankflow is regarded insignificant (fig. 6). Other constraints are (Odgaard, 1986): (1) effective river width is constant; (2) centreline radius of curvature is large compared with width; (3) large width/depth ratio; (4) transverse velocity components are small compared to longitudinal; (5) the turbulence is isotropic. Because it was shown that meandering is not dependent on scale, it is desirable to have the model results independent of scale. Therefore the model will be written in dimensionless terms. Here only a brief summery of the model is given, for a complete description of the model is referred to Odgaard (1986*a*). As the model describes a steady state, the only variables dependent on scale are length and velocity. For both quantities a suitable reference value is present in the model. Both effective width and centreline depth are assumed constant in the model, as well as the averaged centreline longitudinal velocity. As an example, the dimensionless downstream direction $\tilde{s}$ and transverse velocity $\tilde{v}_n$ can be written as:

$$\tilde{s} = \frac{s}{w_e}, \quad s = \tilde{s} w_e \tag{11a}$$

$$\tilde{v}_n = \frac{v_n}{\overline{v}_{sc}}, \quad v_n = \tilde{v}_n \overline{v}_{sc} \tag{11b}$$

were the tilde denotes a dimensionless variable. In the following all length and velocity variables will be treated dimensionless unless stated otherwise and the tilde for these variables will be omitted for clarity.

The starting point of the meander flow model is the equation that describes the longitudinal or streamwise variation of the centreline transverse bedslope (S_{Tc}). This equation is derived from a combination of the equation of

motion for the transverse velocity component, a parabolic eddy viscosity profile, a parabolic velocity profile, the mass balance at the centreline to compensate for mass-shift and a simple linear relationship between the transverse bedslope and the transverse velocity at the bottom. At the centreline of the river this yields (Odgaard, 1986*a*, his equation 30):

$$\frac{d^2 S_{Tc}}{d\tilde{s}^2} + a' \frac{dS_{Tc}}{d\tilde{s}} + b' S_{Tc} = \frac{c'}{\tilde{r}_c} \tag{15}$$

in which

$$a' = \frac{16\kappa h'}{3\alpha\sqrt{\theta}} \frac{m+2}{m+1} \frac{1}{F_{Dc}} \tilde{d}_c \tag{AIII-1a}$$

$$b' = \frac{32\kappa^3 h'}{3\alpha\sqrt{\theta}} \frac{m+2}{(m+1)^2} \frac{1}{F_{Dc}} \tag{AIII-1b}$$

$$c' = \frac{16\kappa^2 h'}{m+1} \tilde{d}_c \tag{AIII-1c}$$

and

$$h' = \frac{2m+1}{2\kappa^2 m} \tag{AIII-1d}$$

The particle Froude number and the velocity profile exponent are defined as:

$$F_D = \frac{\bar{v}_s}{\sqrt{\frac{\rho_s - \rho}{\rho} gD}} \tag{AIII-2}$$

$$m = \kappa \frac{\bar{v}_s}{v_*} = \kappa \frac{C}{\sqrt{g}} \tag{AIII-3}$$

With the downstream change in centreline transverse bedslope given by equation AIII-2, the depth distribution along the width of the river can now be calculated according to (Odgaard, 1986*a*, his equation 48):

$$S_T = S_{Tc} \frac{\tilde{d}}{\tilde{d}_c} \frac{\tilde{r}_c}{\tilde{r}} \tag{16}$$

When interpreting S_T as $d(d)/dr$ this can be written for convenience as (Odgaard, 1986*a*, his equation 49):

$$\frac{\tilde{d}}{\tilde{d}_c} = \left(\frac{\tilde{r}}{\tilde{r}_c} \right)^{\frac{S_{Tc}\tilde{r}_c}{\tilde{d}_c}} \tag{AIII-4}$$

Equation 16 results in a increasing transverse bedslope toward the outer bank. An example of a depth distribution described by equation 16 is given in Figure 6.

Now the depth distribution along the river bend is known, focus is now laid on how to calculate the velocity distributions. The vertical distribution of the longitudinal velocity is given by (Odgaard, 1986*a*, his equation 3, see also Figure 6):

$$\frac{\tilde{v}_s}{\bar{\tilde{v}}_s} = \frac{m+1}{m} \left(\frac{\tilde{z}}{\tilde{d}} \right)^{\frac{1}{m}} \tag{12}$$

In order to calculate the entropy production, only $\bar{\tilde{v}}_s$ has to be known (see appendix IV). The distribution of $\bar{\tilde{v}}_s$ along the river can be determined from the following differential equation (Odgaard, 1986*a*, his equation 15):

$$\frac{d\bar{\tilde{v}}_s^2}{d\tilde{s}} + g' \frac{\tilde{d}_c}{\tilde{d}} \bar{\tilde{v}}_s^2 = g' \frac{\tilde{r}_c}{\tilde{r}} \tag{17}$$

in which

$$g' = \frac{2\kappa^2}{(m+1)^2} \frac{1}{\tilde{d}_c} \tag{AIII-5}$$

The vertical distribution of the transverse velocity is assumed to be linear. Because the main interest lies in the velocity gradients, the (constant) mass shift caused by a change in curvature that is one of the main features of the meander flow model, is not used in this analysis. The distribution of $\tilde{v}_n$ can therefore simply be written as (Odgaard, 1986*a*, his equation 4):

$$\frac{\tilde{v}_n}{\tilde{v}_{ns}} = 2 \left(\frac{\tilde{z}}{\tilde{d}} - \frac{1}{2} \right) \tag{13}$$

in which $\tilde{v}_{ns}$ is the transverse surface velocity (see fig. 6). The transverse surface velocity is the same as the transverse bed velocity (but with opposite sign). Because the transverse bed slope was determined from the concept of transverse force balance on a sediment particle (upward force proportional to transverse bed velocity), the transverse surface velocity can be determined from the simple relationship (Odgaard, 1986*a*, his equation 21):

$$\tilde{v}_{ns} = d' S_T \tag{AIII-6}$$

in which

$$d' = \frac{2}{3\alpha} \frac{\kappa G}{\sqrt{\theta}} \frac{m+2}{m+1} \frac{1}{F_D} \tag{AIII-7}$$

Finally, the dependence of the eddy viscosity on the depth is assumed to be parabolic. In non-dimensionless form:

$$\varepsilon = \kappa v_* z \left(1 - \frac{z}{d} \right) \tag{AIII-8}$$

in which the shear velocity is given by: $v_* = \kappa \bar{v}_s / m$. The first term between brackets is the result of the dimensionless treatment.

APPENDIX IV. ANALYTICAL SOLUTION OF FIRST INTEGRAL OF EQUATION 10

With the velocity distributions (eq. 12 and 13), the expression for entropy production (eq. 10) can be further worked out. Differentiating the vertical longitudinal and transverse velocity distributions yields:

$$\left(\frac{d\tilde{v}_s}{d\tilde{z}}\right)^2 = \tilde{\bar{v}}_s^{\,2}\left(\frac{m+1}{m^2}\right)^2 \tilde{d}^{-\frac{2}{m}}\tilde{z}^{\frac{2}{m}-2} \qquad \text{(AIV-1a)}$$

and

$$\left(\frac{d\tilde{v}_n}{d\tilde{z}}\right) = 4\left(\frac{\tilde{v}_{ns}}{\tilde{d}}\right)^2 \qquad \text{(AIV-1b)}$$

Together with the eddy viscosity profile (eq. AIII-8) these equations can be substituted in equation 10. In order to obtain the entropy production over a cross-section, this equation is integrated over the $\tilde{z}$ - and $\tilde{n}$ -directions. This results in:

$$\frac{T\sigma_{cs}w}{\rho\bar{v}_{sc}^{\,3}} = \frac{\kappa^2}{m}\int_{-\frac{1}{2}}^{\frac{1}{2}}\int_0^{\tilde{d}}\left(\tilde{z}\left(1-\frac{\tilde{z}}{\tilde{d}}\right)\tilde{\bar{v}}_s^{\,3}\left(\frac{m+1}{m^2}\right)^2\tilde{d}^{-\frac{2}{m}}\tilde{z}^{\frac{2}{m}-2} + 4\tilde{\bar{v}}_s\left(1-\frac{\tilde{z}}{\tilde{d}}\right)\left(\frac{\tilde{v}_{ns}}{\tilde{d}}\right)^2\right)d\tilde{z}d\tilde{n} \qquad \text{(AIV-2)}$$

The first integral of this equation can be solved analytically. Rewriting results in:

$$\frac{T\sigma_{cs}w}{\rho\bar{v}_{sc}^{\,3}} = \kappa^2\int_{-\frac{1}{2}}^{\frac{1}{2}}\int_0^{\tilde{d}}\left(\frac{(m+1)^2}{m^5}\tilde{\bar{v}}_s^{\,3}\tilde{d}^{-\frac{2}{m}}\left(\tilde{z}^{\frac{2}{m}-1}-\frac{1}{\tilde{d}}\tilde{z}^{\frac{2}{m}}\right) + \frac{4}{m}\tilde{\bar{v}}_s\left(\frac{\tilde{v}_{ns}}{\tilde{d}}\right)^2\left(\tilde{z}-\frac{\tilde{z}^2}{\tilde{d}}\right)\right)d\tilde{z}d\tilde{n} \qquad \text{(AIV-3)}$$

After integrating and regrouping the entropy production over a cross-section can be written as:

$$\frac{T\sigma_{cs}w}{\rho\bar{v}_{sc}^{\,3}} = \kappa^2\int_{-\frac{1}{2}}^{\frac{1}{2}}\left(\frac{(m+1)^2}{4m^3+2m^4}\tilde{\bar{v}}_s^{\,3} + \frac{4\tilde{\bar{v}}_s\tilde{v}_{ns}^{\,2}}{6m}\right)d\tilde{n} \qquad (14)$$

From equation 14 it can be seen that only the average longitudinal velocity and the transverse surface velocity have to be determined for the entropy production, which means that the model only has to describe these parameters and not the complete velocity distribution. Unfortunately no simple relationships exist which describe $\tilde{\bar{v}}_s$ and $\tilde{v}_{ns}$, so no further analytical solution of equation 14 is possible.

APPENDIX V. SCRIPT TO DETERMINE PARAMETERS FOR THIRD ORDER SINE GENERATED CURVE FOR GIVEN SINUOSITY

```
================================================
% Determineparameters
% This script determines the parameter values of a
3rd order sine generated curve for a fixed
wavelength
% Created on march 6 2002 by Adriaan Teuling
% Copyright by Department of Water Resources,
Wageningen University, The Netherlands
% This script was created in Matlab 5.3.
================================================

%Input
ThetaOmin = 68*(2*pi/360)
deltaTheta = 0.005*(2*pi/360);
ThetaOmax = 100*(2*pi/360)
numberThetaOvalues = (ThetaOmax-
ThetaOmin)/deltaTheta; %has to be whole number

bmin = -0.1;
deltab = 0.01;
bmax = 0.1;
numberbvalues = (bmax-bmin)/deltab+1; %has to be
whole number

dmin = -0.1;
deltad = 0.01;
dmax = 0.1;
numberdvalues = (dmax-dmin)/deltad+1; %has to be
whole number

L = 30;
deltas = 0.1; %step size
numberpoints = L/deltas+1; %has to be whole number
s = 0:deltas:L;
c = 2*pi/L;

wavelength = 13.2;
target = 0.01; %accuracy
%End input

TotalCalculations=numberbvalues*numberdvalues
ThetaO=ThetaOmin:deltaTheta:ThetaOmax;
b=bmin:deltab:bmax;
d=dmin:deltad:dmax;
p=0;
x(1)=0;
A=0;

for l=1:numberbvalues;
    for m=1:numberdvalues;
        for k=1:numberThetaOvalues;
            for o=1:numberpoints-1;

    deviationangle(o)=ThetaO(k)*sin(c*s(o))+ThetaO
(k)^3*b(l)*sin(3*c*s(o))+ThetaO(k)^3*d(m)*cos(3*c*
s(o));

    x(o+1)=x(o)+deltas*cos(deviationangle(o));
            end
            if abs((x(numberpoints)-x(1))-
wavelength)<=target;
                p=p+1
                A(p,1)=ThetaO(k);
                A(p,2)=b(l);
                A(p,3)=d(m);
             A(p,4)=(x(numberpoints)-x(1));
             break
          else
          end
        end
    end
end

save Result A

A %shows the result
```

APPENDIX VI. SOURCE CODE OF MEANDER FLOW MODEL

```
================================================
% MEANDERMODEL version 2.2
% Created on january 14 2002 by Adriaan Teuling
and Schalk-Jan van Andel
% Copyright by Department of Water Resources,
Wageningen University, The Netherlands
% This script was created in Matlab 5.3.
================================================

warning off

A =[1.8511   -0.0200    0.0110];
    % Copy the matrix A (Determineparameters.m)
containing Theta0, b and d for a given channel-
and wavelength

for j=1:1; % Number of rows of matrix A
j % Shows progress of calculation in command
window

% Definition of planform parameters
global L
L = 41; %must be the same as in the calculations
for A
global ThetaO
ThetaO = A(j,1);
global b
b = A(j,2);
global d
d = A(j,3);
global xmax
xmax = 120; %at least max L

% Grid definition
global smin
smin = 0; %must be multiple of deltas
global deltas
deltas = 0.1;
global nmin
nmin = -1/2;
global deltan
deltan = 0.1;
global nmax
nmax = 1/2;

% Initial conditions
global STc0
STc0 = [0.0;0.0];
global uu0
for k=1:1:((nmax-nmin)/deltan+1);
uu0(k) = 1;
end

% Calculation of energy dissipation
Findconstantenergyprofile

% Saying results
B(j,:)=[ThetaO b d VarianceEnergycs count check];
save Result B

end

B %Shows final result matrix


================================================
% Findconstantenergyprofile
% This script runs the meander flow model until
the energy loss is constant
% This script is part of the MEANDERMODEL 2.2
% Created on march 6 2002 by Adriaan Teuling and
Schalk-Jan van Andel
% Copyright by Department of Water Resources,
Wageningen University, The Netherlands
% This script was created in Matlab 5.3.
================================================

global L
global Energy1
Energy1 = 20;
global xmax
global window %must be multiple of deltas
window = round(0.9*L); %determines the size of the
shift after each calculation round.
global reach %Reach/width must be multiple of
deltas
reach = 5*L;
global check
check = 1;
global smin
global deltas
global nmin
global deltan
global nmax
global n
n = [nmin:deltan:nmax];
global STc0
global uu0

for count = 1:1:5; %Maximum number of calculations
for the energy loss to become constant

    Runflowmodel;

    global TotalEnergydissipation
    global Energy1
    z = abs(TotalEnergydissipation-
Energy1)/TotalEnergydissipation; %Relative
difference in energy loss
    if z<0.01
        break
        global check
    elseif check==-1 %check to see if the
calculations converge. If not check becomes -1 but
the calculations proceed.
        break
    elseif count==5 %has to be max count to
prevent shift of s
        global check
        check=-1;
    break
    else %new initial conditions for next
calculation round
        global s
        s = s1+window;
        global STc0
        STc0 = STc(window/deltas+1,:);
        global uu0
        uu0 = uuu(window/deltas+1,:);
        global smin
        smin = min(s);
        global Energy1
        Energy1=TotalEnergydissipation;
    end
end


================================================
% Runflowmodel
% This script executes the different parts of the
meander flow model
% This script is part of the MEANDERMODEL 2.2
% Created on march 6 2002 by Adriaan Teuling and
Schalk-Jan van Andel
% Copyright by Department of Water Resources,
Wageningen University, The Netherlands
% This script was created in Matlab 5.3.
================================================

Calculateriverplanform;

Calculateradiusofcurvature;
global rc
global Rc

Physicalparameters;

Calculatetransversebedslope;
global STc
```

```
Calculatedepth;
global ddd
global drel

Calculatelongitudinalvelocity;
global uuu
global u

Calculatetransversevelocity;
global vs
global vsmax

Calculateenergyparameters;
global TotalEnergydissipation
global Eamplitude
global VarianceEnergycs
global Energy
global Energycs


================================================
% Calculateriverplanform
% This script plots the 3rd order sine generated
curve
% This script is part of the MEANDERMODEL 2.2
% Created on march 6 2002 by Adriaan Teuling and
Schalk-Jan van Andel
% Copyright by Department of Water Resources,
Wageningen University, The Netherlands
% This script was created in Matlab 5.3.
================================================

clear global s
clear global deviationangle
clear global x
clear global y

global L
global ThetaO
global b
global d
global smin
global deltas
global reach
global Border
Border = reach;
global s
s = smin:deltas:Border;
global c
c = 2*pi/L;
global deviationangle
global x
global y
x(1)=0;
y(1)=0;
global xmax

for o=2:1:(Border-smin)/deltas+1;
    check=1;
    ss=s(o-1)+0.25*L;
    deviationangle(o-
1)=ThetaO*sin(c*ss)+ThetaO^3*b*sin(3*c*ss)+ThetaO^
3*d*cos(3*c*ss);
    x(o)=x(o-1)+deltas*cos(deviationangle(o-1));
    y(o)=y(o-1)+deltas*sin(deviationangle(o-1));
    if (x(o)-xmax)>0
        break
    else
    end
end

global smax
smax=(ss-0.25*L)+deltas;
clear global s
clear global s1
global s
s=[smin:deltas:smax]';
global s1
s1=[smin:deltas:smax]';
global channellength
channellength=(smax-smin);

================================================
% Calculateradiusofcurvature
% This script calculates the radius of curvature
as function of s
% This script is part of the MEANDERMODEL 2.2
% Created on march 6 2002 by Adriaan Teuling and
Schalk-Jan van Andel
% Copyright by Department of Water Resources,
Wageningen University, The Netherlands
% This script was created in Matlab 5.3.
================================================

function rc = radius(s,b,c)
clear global rc
global L
global ThetaO
global b
global c
global d
global smin
global deltas
global smax
global s
global rc

for h=1:1:(smax-smin)/deltas+1;
    ss=s(h)+0.25*L;
    if
(c*ThetaO*cos(c*ss))+ThetaO^3*b*3*c*cos(3*c*ss)-
ThetaO^3*d*c*3*sin(3*c*ss)==0;
        rcc(h)=-realmax;
    else

    rcc(h)=1/(c*ThetaO*cos(c*ss)+ThetaO^3*b*3*c*co
s(3*c*ss)-ThetaO^3*d*c*3*sin(3*c*ss));
    end
end

rc=rcc';
global Rc
Rc=min(abs(rc));


================================================
% Physicalparameters
% This script contains the values of most
parameters used in the meander flow model
% This script is part of the MEANDERMODEL 2.2
% Created on march 6 2002 by Adriaan Teuling and
Schalk-Jan van Andel
% Copyright by Department of Water Resources,
Wageningen University, The Netherlands
% This script was created in Matlab 5.3.
================================================

% Input of physical (flow and sediment) parameters
global kappa %von Karman's constant [-]
kappa = 0.4;
global dc %centerline depth [m], under the
assumption d<<width
dc = 0.1;
global FDc %Particle Froude number centerline
FDc = 6.85;
global m %velocity profile exponent (m=mc)[-]
m = 2.8;
global alpha %ratio of projected surface area to
volume for a sediment particle divided by that for
a sphere of the same volume (alpha=1.27 for
ordinary river sand)[-]
alpha = 1.27;
global Theta %Shield's parameter[-]
Theta = 0.04;

global N %constant factor, checked by measurements
N = 2*m+1/(2*kappa^2*m);
global k %proportionality factor, assumed
independent of sediment transport rate
k = kappa*N*(m+2)/(m+1);
global aaa %proportionality factor ST=a*v's [s/m]
```

```
aaa = (3*alpha/2*sqrt(Theta)/k)*FDc;
global aa %constant
aa =
16*kappa*N*(m+2)*dc/(3*alpha*sqrt(Theta)*(m+1)*FDc
);
global bb %constant
bb =
32*kappa^3*N*(m+2)/(3*alpha*sqrt(Theta)*(m+1)^2*FD
c);
global cc %constant
cc = 16*kappa^2*N*dc/(m+1);
global c3 %constant from longitudinal velocity
equation
c3 = (2*kappa^2)/(((m+1)^2)*dc);


==================================================
% Calculatetransversebedslope
% This script calculates the transverse bedslope
at the channel centerline
% This script is part of the MEANDERMODEL 2.2
% Created on march 6 2002 by Adriaan Teuling and
Schalk-Jan van Andel
% Copyright by Department of Water Resources,
Wageningen University, The Netherlands
% This script was created in Matlab 5.3.
==================================================

function solveSTc

clear global STc
global rc
global aa
global bb
global cc
global s
global deltas
global smin
global STc0
global STc

[s,STc]=ode45('Transversebedslopeequation',s,STc0,
[],aa,bb,cc,rc,deltas,smin);


==================================================
% Transversebedslopeequation
% This script solves the differential equation for
the transverse bedslope
% This script is part of the MEANDERMODEL 2.2
% Created on march 6 2002 by Adriaan Teuling and
Schalk-Jan van Andel
% Copyright by Department of Water Resources,
Wageningen University, The Netherlands
% This script was created in Matlab 5.3.
==================================================

function STcp =
Transversebedslope(s,STc,FLAG,aa,bb,cc,rc,deltas,s
min)
STcp=[STc(2);-aa*STc(2)-bb*STc(1)+cc/rc((s-
smin)/deltas+1)];


==================================================
% Calculatededepth
% This script calculates the depth distribution
% This script is part of the MEANDERMODEL 2.2
% Created on march 6 2002 by Adriaan Teuling and
Schalk-Jan van Andel
% Copyright by Department of Water Resources,
Wageningen University, The Netherlands
% This script was created in Matlab 5.3.
==================================================

function ddd=straal(s,n,STc)
clear global ddd

clear global drel
global smin
global smax
global deltas
global dc
global rc
global s
global STc
global n
global nmax
global nmin
global deltan
global aaa
global ddd
global drel

for y=1:1:((nmax-nmin)/deltan+1)
    nn=n(y);
    for x=1:1:((smax-smin)/deltas+1)
        STcc=STc(x,1);
        rcc=rc(x);
        if abs(rcc)>1e+6
            ddd(x,y)=1*(1-STcc*nn/dc)*dc;
        else
            ddd(x,y)=((rcc-
nn)/rcc)^(STcc*rcc/dc)*dc;
        end
    end
end

drel=ddd/dc;


==================================================
% Calculatelongitudinalvelocity
% This script calculates the longitudinal velocity
profile
% This script is part of the MEANDERMODEL 2.2
% Created on march 6 2002 by Adriaan Teuling and
Schalk-Jan van Andel
% Copyright by Department of Water Resources,
Wageningen University, The Netherlands
% This script was created in Matlab 5.3.
==================================================

function solveu2n

clear global uuu
clear global u
global c3
global deltas
global rc
global s
global smin
global smax
global n
global nmax
global nmin
global deltan
global uu0
global uuu
global drel

for y=1:1:((nmax-nmin)/deltan+1)
    nn=n(y);
    drell=drel(:,y);
    [s,uu]=ode45('Longitudinalvelocityequation',s,
uu0(y),[],c3,drell,nn,rc,deltas,smin);
    uuu(:,y)=uu;
end

global u
u=sqrt(uuu);
```

```
================================================
% Longitudinalvelocityequation
% This script contains the differential equation
for the longitudinal velocity
% This script is part of the MEANDERMODEL 2.2
% Created on march 6 2002 by Adriaan Teuling and
Schalk-Jan van Andel
% Copyright by Department of Water Resources,
Wageningen University, The Netherlands
% This script was created in Matlab 5.3.
================================================

function uup =
Longitudinalvelocity(s,uu,FLAG,c3,drell,nn,rc,delt
as,smin)
uup=[-c3*drell((s-smin)/deltas+1)^(-
1)*uu+c3*rc((s-smin)/deltas+1)/(rc((s-
smin)/deltas+1)-nn)];


================================================
% Calculatetransversevelocity
% This script calculates the transverse velocity
% This script is part of the MEANDERMODEL 2.2
% Created on march 6 2002 by Adriaan Teuling and
Schalk-Jan van Andel
% Copyright by Department of Water Resources,
Wageningen University, The Netherlands
% This script was created in Matlab 5.3.
================================================

function vs=ST(s,n,STc)

clear global vs
global smin
global smax
global deltas
global dc
global rc
global s
global STc
global n
global nmax
global nmin
global deltan
global aaa
global drel
global vs
global vsmax

for y=1:1:((nmax-nmin)/deltan+1)
    nn=n(y);
    for x=1:1:((smax-smin)/deltas+1)
        drell=drel(x,y);
        STcc=STc(x);
        rcc=rc(x);
        vs(x,y)=STcc*drell*((rcc-nn)/rcc)^(-
1)/aaa;
    end
end

vsmax=max(abs(vs(:,nmax/deltan+1)));


================================================
% Calculateenergyparameters
% This script calculates a number of energy
dissipation parameters
% This script is part of the MEANDERMODEL 2.2
% Created on march 6 2002 by Adriaan Teuling and
Schalk-Jan van Andel
% Copyright by Department of Water Resources,
Wageningen University, The Netherlands
% This script was created in Matlab 5.3.
================================================

function Energyconsiderations=uvs(s,n,STc)

clear global Energy
clear global Energycs
clear global TotalEnergydissipation
clear global Eamplitude
clear global VarianceEnergycs

global L
global smin
global smax
global deltas
global nmax
global nmin
global deltan
global m
global kappa
global u
global vs
global Energy
global Energycs
global TotalEnergydissipation
global Eamplitude
global VarianceEnergycs

for f=1:1:(L/deltas+1)
    for i=1:1:((nmax-nmin)/deltan+1)
        if i==1

    Energy(f,i)=(kappa^2)*(((m+1)^2*u(f,i)^3)/(4*m
^3+2*m^4)+(4*u(f,i)*vs(f,i)^2)/(6*m))*(1/2)*deltan
;
        elseif i==((nmax-nmin)/deltan+1)

    Energy(f,i)=(kappa^2)*(((m+1)^2*u(f,i)^3)/(4*m
^3+2*m^4)+(4*u(f,i)*vs(f,i)^2)/(6*m))*(1/2)*deltan
;
        else

    Energy(f,i)=(kappa^2)*(((m+1)^2*u(f,i)^3)/(4*m
^3+2*m^4)+(4*u(f,i)*vs(f,i)^2)/(6*m))*deltan;
        end
    end
end

Energycs = sum(Energy');
TotalEnergydissipation = deltas*sum(Energycs);
Eamplitude = max(Energycs)-min(Energycs);
VarianceEnergycs = var(Energycs); %calculates the
variance of Energycs
```

APPENDIX VII. NOTATION

a' function (equation 15)
b' function (equation 15)
C Chezy coefficient
c' function (equation 15)
c_f fattening parameter
c_s skewing parameter
D particle diameter
d local river depth
$\tilde{d}$ dimensionless local river depth
$\tilde{d}_c$ dimensionless centerline depth
E energy
E_i internal energy
e_i internal energy per unit mass
F_D particle Froude number
f' function (equation 18)
g' function (equation 17)
$\boldsymbol{g}$ vector of acceleration due to gravity
g scalar value of acceleration due to gravity
h' function (equation AIII-1b and AIII-1c)
h_α scale factor in direction α
k sinuosity (L/λ)
L meander length measured along river centerline
m velocity-profile exponent
N cross-stream coordinate divided by centerline radius of curvature (n/r_c)
n cross-stream direction
$\tilde{n}$ dimensionless cross-stream direction
p pressure
Q heat
$\boldsymbol{q}$ vector of heat flow per unit mass
q_i direction i
$\tilde{r}$ dimensionless local radius of curvature
r_c centerline radius of curvature
$\tilde{r}_c$ dimensionless centerline radius of curvature
S entropy
s downstream direction
$\tilde{s}$ dimensionless downstream direction
S_T transverse bedslope
S_{Tc} centerline transverse bedslope
T absolute temperature
t time
$\boldsymbol{v}$ velocity vector
v scalar velocity
v_i velocity component in direction i
v_s velocity component in the downstream direction
$\tilde{v}_s$ dimensionless velocity component in the downstream direction
$\tilde{\overline{v}}_s$ dimensionless depth averaged velocity in the downstream direction
$\overline{v}_{sc}$ depth averaged centerline velocity in the downstream direction
v_n velocity component in the cross-stream direction
$\tilde{v}_n$ dimensionless velocity component in the cross-stream direction
$\tilde{v}_{ns}$ dimensionless surface velocity in the cross-stream direction
v_z velocity component in the vertical direction
v_* shear velocity
W work
w river width
w_e effective river width ($\approx w-2d$)
x downvalley direction
x_0 downvalley coordinate of the river centerline
y crossvalley direction
y_0 crossvalley coordinate of the river centerline
z vertical direction
$\tilde{z}$ dimensionless vertical direction
α projected area/volume ratio for sediment particle normalized by that for sphere
β angle between downvalley and cross-stream axis
ε kinematic eddy viscosity
κ Von Karman's constant (0.4)
δ_s unity vector in the downstream direction
δ_n unity vector in the cross-stream direction
δ_z unity vector in the vertical direction
$\delta_{\alpha\beta}$ Kronecker delta
$\boldsymbol{\tau}$ stress tensor
τ_{ij} components of the stress tensor
τ_{nn} normal stress in the cross-stream direction
τ_{ns} shear stress in the downstream direction on a cross-stream plane
τ_{nz} shear stress in the vertical direction on a cross-stream plane
τ_{ss} normal stress in the downstream direction
τ_{sn} shear stress on a downstream plane in the cross-stream direction
τ_{sz} shear stress on a downstream plane in the vertical direction
τ_{zz} normal stress in the vertical direction
τ_{zn} shear stress on the z plane in the cross-stream direction
τ_{zs} shear stress on the z plane in the downstream direction
Θ deviation angle from valley axis
Θ_0 deviation angle of sine-generated curve from valley axis at point of inflexion
λ meander wavelength
Ψ rate of strain tensor
ρ fluid density
ρ_s particle density
θ Shields' parameter (0.27)
σ rate of entropy production per unit volume
σ_{cs} rate of entropy production per unit river length
σ_{tot} total rate of entropy production for meander bend
ϕ phase along the river ($2\pi s/L$)